Seasonal, regional and vertical characteristics of high carbon monoxide plumes along with their associated ozone anomalies as seen by IAGOS between 2002 and 2019

Thibaut Lebourgeois[1,2], Bastien Sauvage[1], Pawel Wolff[3], Béatrice Josse[2], Virginie Marécal[2], Yasmine Bennouna[1], Romain Blot[1], Damien Boulanger[3], Hannah Clark[4], Jean-Marc Cousin[1], Philippe Nedelec[1], and Valérie Thouret[1]

[1]Laboratoire d'Aérologie, Université de Toulouse, CNRS, UPS, Toulouse, France
[2]CNRM, Université de Toulouse, Météo-France, CNRS, Toulouse, France
[3]Observatoire Midi-Pyrénées, Université de Toulouse, CNRS, UPS, 31400 Toulouse, France
[4]IAGOS-AISBL, 98 Rue du Trône, Brussels, Belgium

Correspondence: Thibaut Lebourgeois (thibaut.lebourgeois@aero.obs-mip.fr)

In-situ measurements from IAGOS are used to characterise extreme values of carbon monoxide (CO) in large regions of the globe in the troposphere between 2002 and 2019. The SOFT-IO model, combining the FLEXPART lagrangian dispersion model with emission inventories over the footprint region is used to identify the origins of the CO in the sampled plumes. The impact of biomass burning and anthropogenic emissions on such CO plumes are characterised through CO mixing ratios and simultaneously recorded ozone (O_3) ones.

In the Northern Hemisphere, CO reaches its maximum values in DJF in the lower troposphere, which can be attributed to elevated anthropogenic emissions and reduced convective activity during the season. Due to the low photochemistry and the fresh age of the air masses the O_3 values of these plumes are low. CO plumes in the upper troposphere result from intense emissions and efficient vertical transport, peaking during JJA. The largest values of CO in the northern hemisphere are found in Eastern Asia in the lower and middle troposphere and in Siberia in the upper troposphere.

Among the anomalies detected in the upper troposphere in JJA, the ones with the higher associated O_3 values are the ones associated with biomass burning emissions. The middle troposphere is a combination of the characteristics of the LT and the UT, with contributions from both local emissions and long-range transport. Among the studied regions, the troposphere above Middle-East and the UT of Siberia presented extremely high O_3 values.

Indian CO anomalies have different characteristics depending on the season as the wet and dry phases of the monsoon have a strong impact on the transport of the pollutant in this region.

Similarly the shift of the inter-tropical convection zone strongly impacts the seasonality of the emissions and the transport patterns above Africa. In that region convection is no longer the limiting factor and the transport of the CO plumes is driven by the ITCZ shift, trade winds and the upper branch of the Hadley cell redistributing the pollution to higher latitudes.

1 Introduction

Extreme weather can sometimes be incorrectly reproduced and predicted by the global and regional models (e.g. Shastri et al. (2017); Lavaysse et al. (2019)). Extreme pollution events can also be difficult to predict, as they can be explained by multiple factors such as abnormal weather conditions and/or unusually intense emissions (either from anthropogenic or natural sources, or both). Hence, it is essential to better understand the distributions of pollutants or their precursors in the atmosphere under such circumstances, leading thus to a better representation by the models and an improvement of their ability to predict their peak values. Among the short-lived climate forcers, tropospheric ozone (O_3) is a key component of our atmosphere, and carbon monoxide (CO) is one of its main precursors. First, O_3 is a pollutant dangerous for human life (Chen et al., 2007; Liu et al., 2018) and for crops (Fuhrer et al., 1997; Davison and Barnes, 1998; Ashmore, 2005). Secondly, it is a trace gas with major influence on the oxidative capacity of the atmosphere as it is the main source of hydroxyl radicals in the troposphere (Seinfeld and Pandis, 2008). Finally, it is a greenhouse gas (GHG) with a positive radiative effect in the troposphere. Moreover multiple studies have shown the upper troposphere-lower stratosphere (UTLS) to be the region with the largest changes in radiative effect from changes in O_3 mixing ratio (Riese et al., 2012; Xia et al., 2018). O_3 can hence have an impact on air quality as much as on climate. This compound in the troposphere is photochemically produced from NOx and Volatile Organic Compounds (VOC) or CO (Seinfeld and Pandis, 2008). Hence, a good estimation of its chemical precursors as well as better understanding of the processes leading to their distributions at global scale are of prime importance.

For these reasons, this study is focused on analysing the most intense anomalies of CO throughout the troposphere over different regions of the world and how O_3 distributions behave in such plumes.

Apart from being a precursor of O_3, CO is also one of the biggest sinks of hydroxyl radical (Lelieveld et al., 2016) and thus has an impact on the oxidative capacity of the atmosphere which can lead to increased lifetimes of other greenhouse gases such as CH_4. Moreover, the oxidation of CO produces greenhouse gases like O_3 and CO_2. CO is hence believed to cause an indirect positive radiative forcing (IPCC, 2013). Finally, CO is a good tracer for pollution export pathways thanks to its long chemical lifetime in the troposphere of a few weeks in summer to a few months in winter (Lelieveld et al., 2016).

CO is mostly emitted in the planetary boundary layer (BL) and can be removed via different mechanisms. These mechanisms highly depend on the regions and seasons. Convective activity represents an significant part of the pollution export pathways from the BL. Some regions are more prone than others to exporting pollutants. Tropical regions have permanent convective activity due to the close proximity of the Inter-Tropical Convergence Zone (ITCZ) (Andreae et al., 2001; Lannuque et al., 2021). Regions like south and eastern Asia benefit from the different phases of the monsoon season (Ricaud et al., 2014; Kar et al., 2004; Park et al., 2007; Lawrence, 2004a) or cold front and warm conveyor belts activity (Liang et al., 2004; Ding et al., 2009; Dickerson et al., 2007). North American pollution is mostly exported through cold front and warm conveyor belts (Owen et al., 2006; Cooper and Parrish, 2004). CO from biomass burning in boreal regions can be emitted directly above the BL and as high as the upper troposphere (UT) through pyroconvection whereas, tropical fires emit mainly in the lower troposphere (Rémy et al., 2017; Val Martin et al., 2010; Damoah et al., 2006). Once in the free troposphere, CO is transported via westerlies or jet streams and can be rapidly transported across the hemisphere (Stohl, 2001; Stohl et al., 2002) and influence the atmospheric

composition of a downwind continent (Liang et al., 2004; Cooper et al., 2004). In special cases, heavily polluted air masses can reach the UT (e.g. Nedelec et al. (2005)). Those events happen when polluted air masses are transported upward by strong (pyro-)convective episodes and can have a relatively large impact on the chemistry in the UT.

CO is a precursor to O_3 with a chemical lifetime long enough to reach the UT, so in this part of the atmosphere CO is hence believed to have an impact on O_3 mixing ratio as long as reservoirs for NOx are available (Seinfeld and Pandis, 2008).

Moreover, large values of CO in the UT are an indication of surface influenced air masses potentially rich in many pollutants, which illustrates the importance of better understanding phenomena able to bring vast amounts of CO in the upper part of the troposphere.

Studies on the export of large quantities of CO in the free troposphere or above have been facilitated with the access to satellite data. An important number of studies have been focused on the eastern/southern part of Asia and especially on the export of the CO emitted into different regions (e.g. Fadnavis et al. (2011); Barret et al. (2016); Smoydzin and Hoor (2022)). Barret et al. (2016) used data from IASI onboard MetOp-A satellite in order to analyse the provenance of the pollution in the upper tropospheric South Asian Monsoon Anticyclone (SAMA) and showed that emissions from the Indo-Gangetic plain were uplifted during the Asian summer monsoon and trapped in its upper level anticyclone. Smoydzin and Hoor (2022) recently used MOPITT to investigate large CO anomalies in the North Pacific and attributed those extremes to emissions from East Asia. Some studies have used the IAGOS database to analyse the characteristics of CO and O_3 values in the troposphere and lower stratosphere. This is the case for Cohen et al. (2018), who used this dataset to study the climatology and trends in O3 and CO in the UTLS. Petetin et al. (2018b); Lannuque et al. (2021); Tsivlidou et al. (2022) used IAGOS to study the characteristics of CO in different regions or altitude layers of the world. Tsivlidou et al. (2022) studied CO and O3 characteristics in the tropical regions. She highlighted the origins of the CO in the different regions of the tropics. She especially showed the importance of the Anthropogenic emissions to explain the values of CO in the tropical troposphere. Lannuque et al. (2021) studied the meridional distribution of O3 and CO over Africa using IAGOS and the satellite IASI (Infrared Atmospheric Sounding Interferometer). They showed the importance of the ITCZ and the upper branch of the Hadley cell for the redistribution of the pollutants over Africa. The Pollutant emitted at the surface is transported by trade winds toward the ITCZ where it is transported to the UT and redistributed to higher latitude by the Hadley cell. Petetin et al. (2018b) studied the CO vertical profile over different airport clusters. They characterised their seasonal profile as well as the seasonality of the highest CO anomalies (95 and 99 percentiles). They showed a strong seasonal variability of the most extreme anomalies in northern America which were due to BB emissions. He also looked at the origins of the CO responsible for the CO anomalies at the different airport clusters.

This emphasises the importance of transport when studying CO extremes in remote parts of the atmosphere. Most of the studies cited above focused on the export of plumes of high CO mixing ratios in one region at a certain altitude and only a few of them were focused on the most extreme CO anomalies. IAGOS (In-service Aircraft for a Global Observing System; http://www.iagos.org) is a European research infrastructure using commercial aircraft in order to measure the atmosphere composition. Thanks to the IAGOS database, we benefit from a large, and long-term in-situ sampling of the atmosphere, complementing the dedicated field campaigns and more global satellite datasets.

The goal of this paper is to characterise the seasonal, regional and vertical CO mixing ratios anomalies for different regions over the globe for almost 20 years as seen by IAGOS along with the simultaneously recorded O_3 between 2002 and 2019. The analysis will explore CO anomalies and their source type (anthropogenic vs biomass burning) and region of emission (14 defined regions of the Global Fire Emissions Database (GFED) (Giglio et al., 2013)). It aims at characterising the distributions and origins of extreme events of polluted plumes in terms of (i) mixing ratios of CO and O3, (ii) frequency and seasonality at different altitudes. O_3 values are presented as additional information, characterising thus the average O_3 content in those plumes of extreme CO. Note that detailed analysis of the O_3 values is outside the scope of the current paper. Such characteristics will form a set of diagnostics that are of particular importance to further test the ability of the models to reproduce extreme events and their impact on the distributions of CO and O_3 throughout the troposphere.

2 Methods and materials

2.1 IAGOS dataset

The data used in this study is from the European research infrastructure IAGOS (Petzold et al., 2015; Thouret et al., 2022)), which has measured different trace gases, particles and meteorological components from passenger airplanes over several decades. IAGOS builds on the experience of the MOZAIC programme (Marenco et al., 1998), which was originally set up in 1994. O_3 and water vapour were the initial compounds measured, with CO measurements added in December 2001. O_3 and CO are measured with an UV and infrared absorption photometer respectively (Thouret et al., 1998; Nédélec et al., 2015), with a total uncertainty of $\pm$ 2 ppb $\pm$ 2% for O_3 and $\pm$ 5 ppb $\pm$ 5% for CO with a time resolution of 4 seconds and 30 seconds respectively. IAGOS took over from MOZAIC in 2011, including an overlap period between 2011 and 2014 (Petetin et al., 2016). The IAGOS European Research Infrastructure also includes the predecessor complementary program CARIBIC (Brenninkmeijer et al., 1999). The consistency between the MOZAIC, IAGOS and CARIBIC datasets are regularly checked following the methodology of Nédélec et al. (2015) and Blot et al. (2021) to ensure the internal consistency of the CO and O_3 measurements since 1994.

As this study focuses on CO and O_3, the dataset used is from the start of the CO measurement (January 2002) to December 2019. This dense network of measurements allows an unprecedented number of pollution events to be sampled for an in-situ dataset with a higher vertical resolution than satellite datasets. In total, more than 43 000 flights were performed by the different aircraft during this period. These flights were performed by 10 different airlines allowing the in situ measurements in several regions of the world. In addition, each flight takes two vertical profiles (during take-off and landing). In contrast with other in-situ datasets from field campaigns, IAGOS is not dedicated to the study of a single phenomenon but rather to the long-term sampling of the atmosphere. This makes the large and precise IAGOS data set particularly suitable for a thorough analysis of the variability of the CO anomalies (see section 2.3.2 for the formal definition) in the different parts of the troposphere.

2.2 SOFT-IO, The source-receptor link

Since IAGOS is not a research project focused on the study of one phenomenon of the atmosphere, but a global exploratory observing system sampling the atmosphere regardless of its current state, a tool was needed to get information on the type of source influencing the air mass (biomass burning or anthropogenic emissions). This is the main usage of the SOFT-IO model.

SOFT-IO is described in detail in Sauvage et al. (2017) and used in scientific studies (e.g. Petetin et al. (2018b); Lannuque et al. (2021); Cussac et al. (2020); Tsivlidou et al. (2022)) so only a broad description of the model is given here. SOFT-IO is a model based on FLEXPART (Stohl et al., 2005) and emission inventories of anthropogenic and biomass burning sources (described below) along the IAGOS flight tracks. A 20-day back trajectory is coupled to the emissions inventories to calculate the CO contributions from recent emissions. The model uses wind fields from ERA interim with a horizontal resolution of $1^\circ \times 1^\circ$ and 137 vertical levels.

The biomass burning inventory used in this version of SOFT-IO is the 1.2 version of the Global Fire Assimilation System (GFAS) (Kaiser et al., 2012). The horizontal resolution is $0.1^\circ \times 0.1^\circ$ with a daily temporal resolution. The emission top altitude is provided by GFAS (v1.2), and is calculated using the fire plume rise model (Paugam et al., 2015; Rémy et al., 2017). GFAS was chosen for its temporal resolution as well as its ability to model emission height. The anthropogenic emissions are from the Community Emissions Data System (CEDS) (McDuffie et al., 2020) with a resolution of $0.5^\circ \times 0.5^\circ$ and a monthly temporal resolution.

SOFT-IO models the CO source contributions and the geographical origin of the emitted CO. The geographical origin of the modelled CO is defined by the same 14 regions as defined in the GFED project (see Fig.1). These contributions cannot be directly compared with observations because SOFT-IO only models contributions from recent emissions (and not older contributions nor the background mixing ratio). SOFT-IO is therefore used here as a qualitative tool to assess whether the modelled contributions are mainly due to anthropogenic or biomass burning emissions and to label the corresponding observed plume as such.

Sauvage et al. (2017) and Tsivlidou et al. (2022) made a thorough statistical evaluation of SOFT-IO. The model had a really good score in the detection frequency of the CO anomalies (above 93% on average). Detection frequency was at its maximum in the LT as most anomalies are from local emissions at this altitude. In the MT and UT, the scores were lower but remained above 80% as the simulation of horizontal and vertical transport could suffer some errors. It is important to note that the study presented here aims at using SOFT-IO only as a qualitative tool to attribute a source type and a relative geographical origin to the emissions leading to the detected anomalies. SOFT-IO is a model which has already been used in several studies similar to the current study (e.g Petetin et al. (2018b); Cussac et al. (2020); Lannuque et al. (2021); Tsivlidou et al. (2022)).

In addition to the various observed parameters and to the SOFT-IO products, the IAGOS data centre provides some meteorological fields from the ECMWF operational analysis interpolated along the IAGOS flight track, as ancillary data (https://doi.org/10.25326/3) . Among these parameters (potential temperature, planetary boundary layer height potential vorticity), the potential vorticity (PV) is used to define whether the CO observations are above or below the dynamical tropopause (defined at 2PVU as in Thouret et al. (2006); Cohen et al. (2018)).

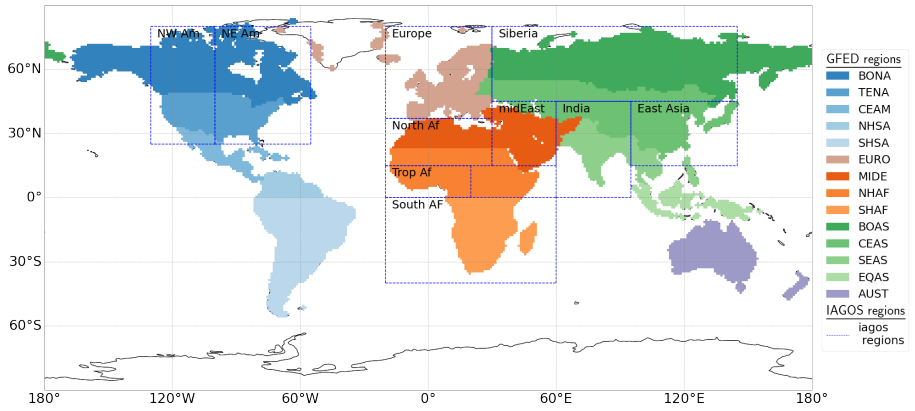

Figure 1. Map of the IAGOS regions (dotted lines) and the GFED defined regions (in colour) (see table A1 in the appendix for the full names of the acronyms).

2.3 Methods

2.3.1 Regions and seasons

In order to synthesise the seasonal and regional characteristics of the CO anomalies, the observations from IAGOS are split into different regions. These regions are defined to be characteristic of specific meteorological and chemical regimes (sources of precursors) similar to Cohen et al. (2018). This study is dedicated to the higher values of the CO distribution, so the sizes of the regions are larger here in order to increase the number of data points per region and not miss any extreme events. By nature, as IAGOS uses commercial aircraft to sample the atmosphere, the different regions are not sampled equally over the same time period (see Fig.B1), but a minimum of 1500 flights per region over the full sampling period is required.

Fig.1 shows the 10 regions defined and used in this study (dotted lines). In addition, the colours of the map indicate the regions as defined by GFED which are used to assign an origin to the emitted CO (see 2.2 and see table A1 in the appendix for the full names of the acronyms). Fig.B2 in the appendix shows the IAGOS flight-tracks of the 18 years of data. It is important to keep in mind that we are studying data from aircraft measurements so they follow specific trajectories. Fig.B3 in the appendix shows the position of each of the visited airport by IAGOS aircraft. The lower and middle troposphere are sampled by IAGOS during landing and takeoff of the aircraft so in proximity of these airports. Note that the average horizontal distance between airport surface and the 8 km altitude is about 300 km (Petetin et al., 2018a). Fig.B1 in the appendix shows the availability of the data in each region. The number of flights is maximum over Europe due to the history of IAGOS and the dense traffic between the US and Europe. However, since 2006, regular flights from Europe to South Africa have been added. In addition, regular flights to eastern and equatorial Asia have been added since 2012.

In the northern hemisphere mid-latitudes (NW Am, NE Am, Eur, Sib and E Asia), four periods of three months are defined according to the meteorological seasons (DJF, MAM, JJA, SON). Note that this study focuses only on the boreal summer and winter periods, one characterising the maximum of CO due to anthropogenic emissions in winter and the other one the

maximum of forest fire activity in summer (section 3.1). The two transitional periods are not presented here as we intend to highlight the influence of the biomass burning emissions on the CO signal. In Africa, the seasons are defined according to the shift of the ITCZ and the rainy seasons (as defined in Lannuque et al. (2021)) : DJFM and JJASO. The results for the two transitional periods (April-May and November) are not presented here. For the Middle-East, seasons of interest for this study are defined the same way as for Africa, because DJFM and JJASO there, also correspond to the maximum and minimum of the CO seasonal cycle, respectively (Figs.C1 and C2). Furthermore, the Middle-East is connected to Africa in terms of emissions as seen in Fig.1 (section 3.3). India (as defined Fig.1) is also an interesting region regarding the different influences of biomass burning and anthropogenic emissions from the different continents. Differently from Northern mid-latitudes and Northern Africa or Middle-East, the four seasons will be discussed here for India (section 3.2).

Finally, in order to characterise these CO extremes at different altitudes, the data sets are divided into three vertical layers.

- Lower Troposphere (LT): from the surface to 2000 m.
- Middle Troposphere (MT): from 2000 m to 8000 m.
- Upper Troposphere (UT): Above 8000 m and below the dynamical tropopause (defined as 2 PVU like in Thouret et al. (2006); Cohen et al. (2018)).

IAGOS samples the lower and free troposphere during the landing and take-off. Petetin et al. (2018a) showed that close to the surface, the IAGOS measurements are representative of urban areas and provide similar measurements to urban background stations. At higher altitudes, in the free troposphere, the samples are less influenced by local emissions and therefore are representative of regional background conditions following the flight tracks shown in Fig.B2 in the appendix.

2.3.2 Definition of the CO anomalies

Fig.2 illustrates the detection of two plumes in the IAGOS observations. The CO anomalies are defined as CO values exceeding the threshold for three consecutive measurements (i.e. a distance of approximately 3 km during cruise phase). The chosen threshold used in this study is the 95th percentile (q95) calculated for each region/season/altitude range (see table 1). Depending on the altitude layer between 49 and 2186 anomalies have been observed per region/season/altitude layer (table A4).

SOFT-IO is then used as a qualitative tool to assign a source type to each of the detected anomalies. This diagnostic is only applied if the contributions modelled by SOFT-IO are above a detection threshold defined as 5 ppb. Several thresholds were tested during this study and did not have a significant impact on the results. According to the method used in Petetin et al. (2018b) the four categories are defined as follow :

- Anthropogenic: if the anthropogenic contributions calculated by SOFT-IO are at least twice those of the biomass burning.
- Biomass burning : if the biomass burning contributions calculated by SOFT-IO are at least twice the anthropogenic contributions.
- MIX sources: if none of the contributions, as calculated by SOFT-IO, is twice the other.

		LT	FT	UT
NW Am	DJF	256	160	146
	MAM	255	170	171
	JJA	251	149	145
	SON	243	141	120
NE Am	DJF	264	159	126
	MAM	246	166	156
	JJA	241	156	132
	SON	241	140	112
Eur	DJF	332	158	126
	MAM	267	164	140
	JJA	200	140	123
	SON	253	138	109
Sib	DJF	no data	no data	127
	MAM	no data	no data	146
	JJA	no data	no data	181
	SON	no data	no data	123
E Asia	DJF	559	209	129
	MAM	504	265	185
	JJA	441	173	162
	SON	457	180	159

		LT	FT	UT
India	DJF	424	157	132
	MAM	305	191	130
	JJA	267	134	131
	SON	470	150	150
North Af	DJFM	no data	no data	145
	AM	no data	no data	156
	JJASO	no data	no data	110
	N	no data	no data	124
Middle E	DJFM	253	148	135
	AM	272	143	131
	JJASO	300	129	113
	N	244	127	118
Gulf of G	DJFM	724	297	190
	AM	419	203	171
	JJASO	280	192	147
	N	383	199	155
South Af	DJFM	219	132	172
	AM	272	120	148
	JJASO	400	245	197
	N	247	150	153

Table 1. q95 values (in ppb) used as thresholds for the different regions for different seasons. For North Africa and Siberia no airports are visited by IAGOS aircrafts so there is no data available for the MT and LT layers.

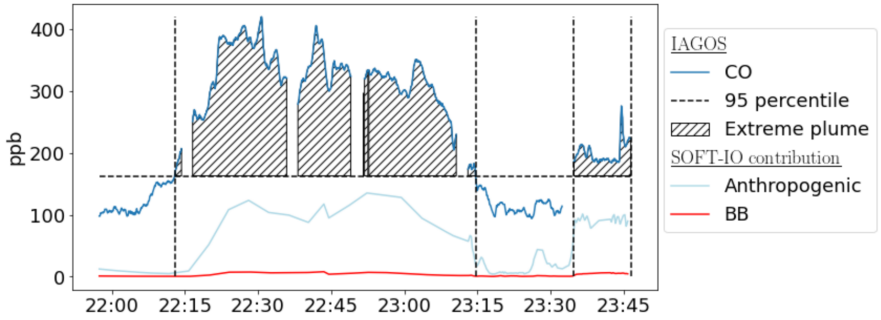

Figure 2. Illustration of the method used to define the CO anomalies applied to part of a IAGOS flight (data here are taken over Siberia at cruise altitude (around 250 hPa) the 7th of June 2013). The dark blue line represents the CO measured by IAGOS. The horizontal dashed line represents the seasonal and regional 95th percentile of the IAGOS dataset (181 ppb). It is used as the threshold for the CO anomalies in this region and season, at this altitude level (UT). The hatched area represents the defined anomalies. The light blue and red lines represent the modelled anthropogenic and biomass burning contributions modelled by SOFT-IO. The gaps are missing data.

– Observed by IAGOS but undetected by SOFT-IO.

In Fig.2 both plumes of high CO mixing ratios are clearly attributed to anthropogenic sources. In addition, SOFT-IO provides information on the emitting region of the contributions (see section 2.2). This diagnosis is repeated for each plume detected. Thus, we can compute the main emitting region responsible for all detected plumes.

3 Results:

The first part of the results is dedicated to the five regions in the northern hemisphere mid-latitudes (NW and NE America, Europe, Siberia and East Asia), then India, and Africa (North Africa, the Gulf of Guinea and South Africa) plus the Middle-East. Each vertical layer will be treated individually from the lower troposphere (LT) to the upper Troposphere (UT) (Siberia and North Africa are only sampled in the UT). The characteristics of the CO-extreme plumes will be given before presenting the associated O_3 distributions in such plumes.

3.1 Northern hemisphere mid-latitudes

3.1.1 Lower troposphere (LT)

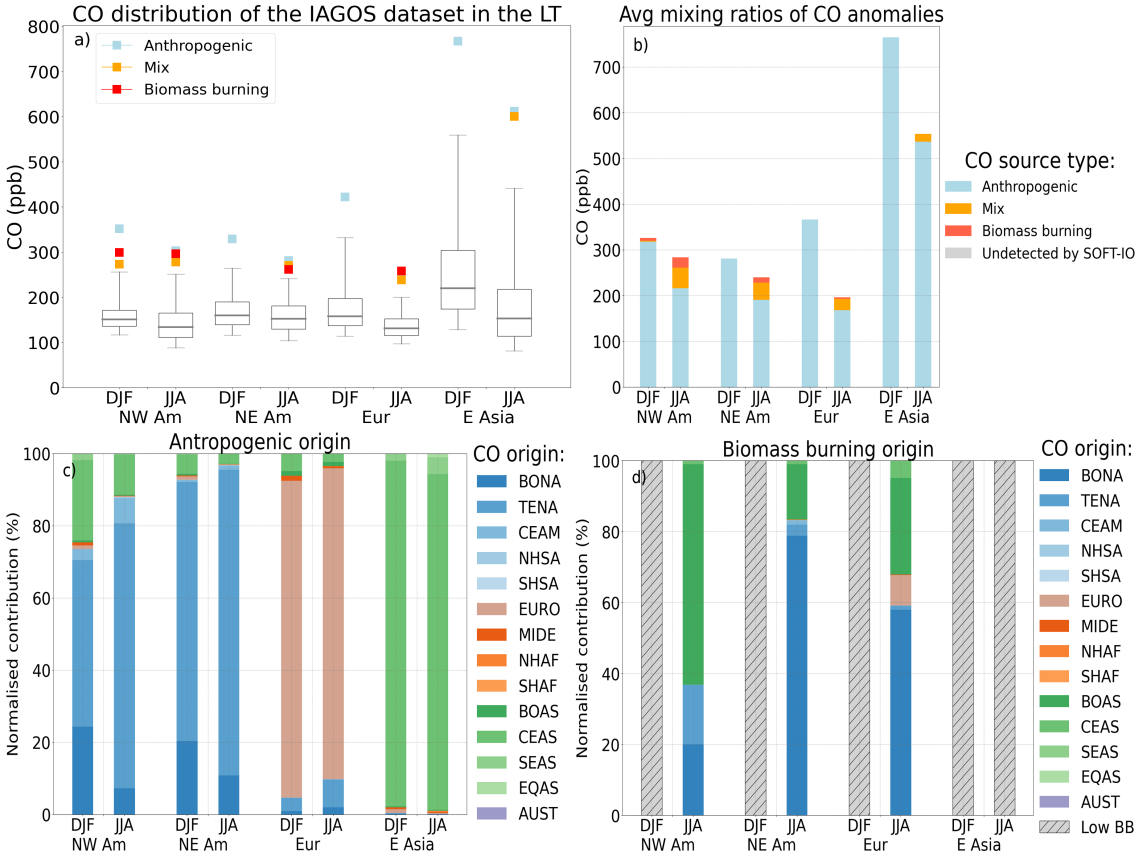

Figure 3. a) CO measured by IAGOS in the LT (below 2km). The box-plot represents the 5th, 25th, 50th, 75th and 95th percentiles of the CO distribution, while the coloured squares represent the mean values of CO inside the detected anomalies (each colour represents a type of CO anomaly attributed to a different source with SOFT-IO: red for biomass burning, blue for anthropogenic and orange for MIX sources). b) Bar-plot showing the averaged mixing ratios of CO in all the detected anomalies (>q95) in the LT in each region for JJA and DJF (given by the total height of the bar), and their proportion according to the different sources (blue for anthropogenic, red for biomass burning and orange for mix, the relative height of the coloured blocks represents the proportion of each type of anomalies). The proportion of plumes where no contribution is modelled by SOFT-IO are represented in grey (in this figure no anomalies are undetected by SOFT-IO over the 4804 observed). c) Regional origin (according to GFED regions, as in Fig. 1) of the anthropogenic contributions of the anomalies associated with MIX and anthropogenic sources in the LT in NH extra-tropics (the hatched part cover region/season with not enough anomalies attributed to the MIX or anthropogenic categories) d) Same for the origin of the biomass burning contributions associated with MIX and biomass burning anomalies. The Low BB patched (hatched grey patches) is applied if a regions has less than 3% of its plumes attributed to either MIX or BB sources.

In the LT (Fig.3) of most regions, the distribution of CO is higher in DJF than in JJA due to the higher anthropogenic emissions during the winter months (e.g mean of the anthropogenic emissions from CEDS in Europe are 60% higher in DJF than in JJA).

The higher levels of CO near the surface in winter are also due to the weak convection and mixing in this season, which allows pollutants to accumulate in the boundary layer (Cohen et al., 2018), and its longer chemical lifetime due to the lower photochemistry during this season (Novelli et al., 1998).

IAGOS observation are in the LT similar to urban background stations (Petetin et al., 2018a). So as expected, anthropogenic contributions have a strong local influence in this layer (Fig. 3.c). For example, anthropogenic contributions are almost entirely from local sources in NW America, NE America and Europe in the LT. Inter-continental transport generally needs no more than a few days in the in the middle troposphere of the northern hemisphere because of the strong prevailing winds there (Jaffe et al., 1999; Liang et al., 2007). Polluted airmasses can also be transported for long distances at lower altitudes, or sink in the Boundary layer (BL) after being transported at higher altitudes, but it generally requires a few additional days (Stohl et al., 2002). Most of the European pollution is exported via low altitude pathways, and can impact the concentration of CO in the LT of Eastern Asia North America and Northern Africa (Huntrieser and Schlager, 2004; Duncan et al., 2008; Li et al., 2002). However those contributions in North America and East Asia are generally low compared with the mixing ratio of CO in the LT of those regions. Here, we are interested in the extreme values at the surface close to the major airports of the region (and therefore close to urbanised areas) so the low contributions from Europe are of minor importance but could have more impact in remote parts of Asia.

In DJF, as there are almost no fires in the northern hemisphere mid-latitudes, almost all of the CO anomalies are attributed to anthropogenic emissions.

In JJA, even if they remain rare, some regions have a few of their anomalies attributed to Biomass Burning (BB) emissions, which are mostly from boreal regions. Even in Europe, where more than half of the BB contributions of the MIX and BB anomalies are from boreal North America.

In the LT, the highest values of CO are found in Eastern Asia during both seasons. The anomalies can even reach a mixing ratio over 700 ppb in DJF. Those extremely high values are due to the emissions from local anthropogenic sources and especially from the industrial and residential sectors (Qu et al., 2022).

As outlined in the introduction, CO is an interesting tracer for surface influenced airmasses, but also because it is a precursor of O_3. It is therefore important to also analyse the O_3 mixing ratio within the detected CO plume. This is shown in Fig.4. The figure shows the seasonal distribution of O_3 measured in the 18 years of data to the values of O_3 measured in the different types of CO anomalies.

In the LT in DJF, our results are similar regardless of the region. We observe values of O_3 inside the CO anomalies close to the minima of the seasonal O_3 cycle. We can see that, in addition to the low photochemical activity linked to the boreal winter, we are seeing a cycle of O_3 destruction in the CO-rich fresh airmasses. These low values of O_3 in polluted urban airmass are often characteristic with NO titration (e.g. Yang et al. (2019)). In JJA, the mean O_3 mixing ratios in the CO anomalies are closer to the median. However, there are strong regional variations showing the significant local influence at this altitude. East

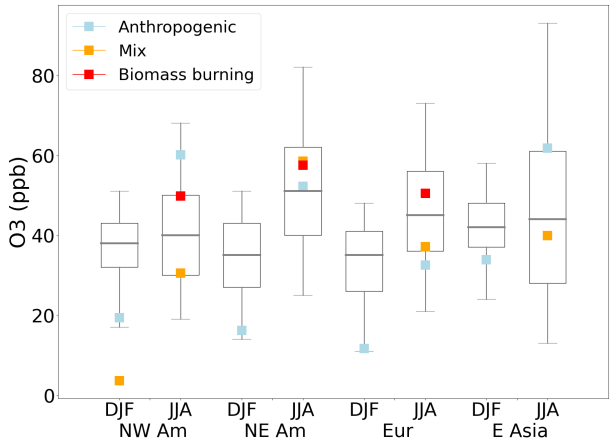

Figure 4. O_3 distribution measured by IAGOS in the lower troposphere (LT) (from the surface to 2000m). Coloured points represent O_3 mixing ratios inside the detected CO anomalies (each colour represents a type of CO anomaly attributed to a different source with SOFT-IO). The box plot represents the 5th, 25th, 50th, 75th and 95th percentiles of the O_3 distribution of the complete database (of these regions, seasons and vertical layer) during the studied period with the simultaneous CO records.

Asia is a region with significant O_3 values and a region having frequent high O_3 episodes (Chang et al., 2017b; Lu et al., 2018). In this region anthropogenic CO anomalies are also associated with elevated O_3 values (20 ppb above the median).

3.1.2 Middle Troposphere (MT)

At higher altitudes, the measured CO is less influenced by the local conditions and emissions. This altitude layer is more impacted by long-range transport as the strong westerly winds present in the free troposphere (middle and upper troposphere) allow a rapid transport of the polluted airmasses across the northern hemisphere mid-latitudes. (Jaffe et al., 1999; Stohl et al., 2002; Liang et al., 2007).

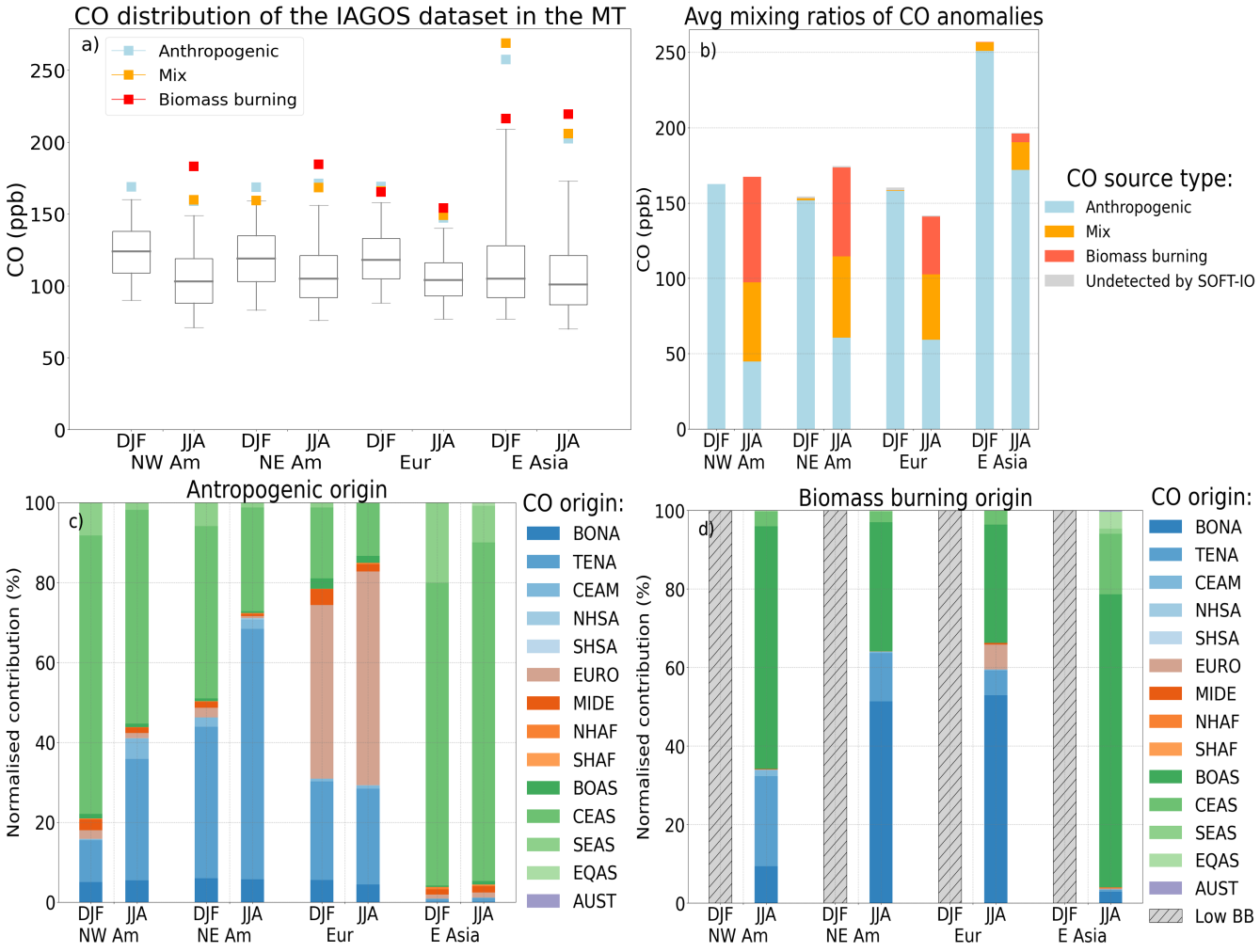

Figure 5. Same as Fig.3 but for the MT (between 2000m and 8000m). At this altitude 24 anomalies over the 5341 observed, are undetected by SOFT-IO, representing thus 0.4% (in grey on panel b).

In the MT (Fig.5), the CO distribution presents a maximum in DJF. In this layer of the atmosphere, the local influence in the anthropogenic contributions is still strong (Fig.5.c). Well known efficient processes for long-range transport of pollution are the Warm Conveyor Belts (WCB) and frontal systems (e.g. (Cooper et al., 2004; Ding et al., 2009)) which can transport polluted surface airmasses to higher altitudes where strong winds (e.g. jet stream at mid-latitude) can rapidly transport those airmasses to another continent. So, in general, there is significant export of the pollutant from the regions at the western part of an ocean (start of the WCB) and the continent in the eastern part of the ocean will be the receptor (Europe and Western America) (Stohl et al., 2002; Huntrieser and Schlager, 2004; Cooper and Parrish, 2004). This feature is well captured by SOFT-IO where we can see that a significant part of the contribution in NW America is coming from Eastern Asia. It is also true for Europe where more than half of the contributions are coming from either North America or Asia. We can also see the lower contribution from

long range transport in summer when the WCB is weaker (Cooper and Parrish, 2004). East Asia is mostly impacted by its own pollution during the two seasons. The upwind continent is Europe and there is no efficient vertical transport pathways over this continent. Therefore, it is not prone to export its pollution. By contrast, East Asia is one of the regions with the most efficient vertical transport (Stohl et al., 2002).

In JJA, BB contributions come mostly from boreal America and Asia. Most of the time, the airports sampled by IAGOS are further south than most of the intense boreal fires. So, it is not surprising that little influence of the BB is detected in the LT. However, the influence from BB grows with altitude. In the MT, we observe an increased number of episodes attributed to either BB emissions or MIX sources in the MT of America and Europe in JJA (Fig.5.b). Fig.5.a shows that the plumes attributed to BB emissions are the most intense in JJA.

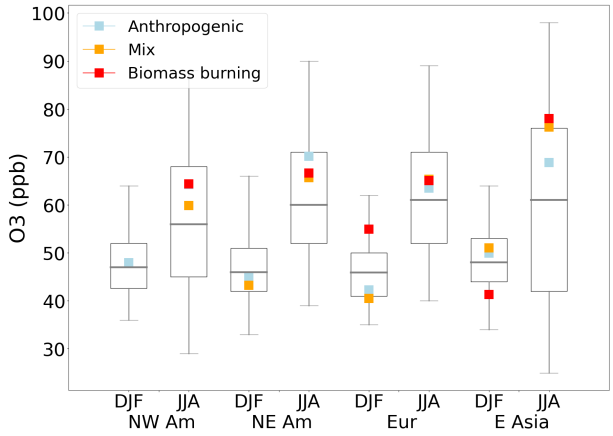

Figure 6. Same as Fig.4 for the MT.

Fig.6 shows the mixing ratio of O_3 associated with high values of CO. In the MT, there is almost no signal during the winter months (mixing ratio of O_3 inside CO anomalies is close or below the median) because of the relatively weak photochemical activity. In JJA, the O_3 mixing ratio within the CO anomalies is between the median and the 75th percentile of the total O_3 distribution, so the mixing ratio of O_3 in the CO plume are on average 5 to 10 ppb higher than the median values depending on the region. In East Asia, BB (and MIX) plumes are rare and mostly come from boreal North Asia. O_3 values within those plumes are 20 ppb higher than the median and 10 ppb higher than the plumes from anthropogenic emissions.

3.1.3 Upper troposphere

To reach the UT, a polluted airmass needs to meet with an intense vertical transport episode but, when in the UT, those airmasses can rapidly cross the entire hemisphere.

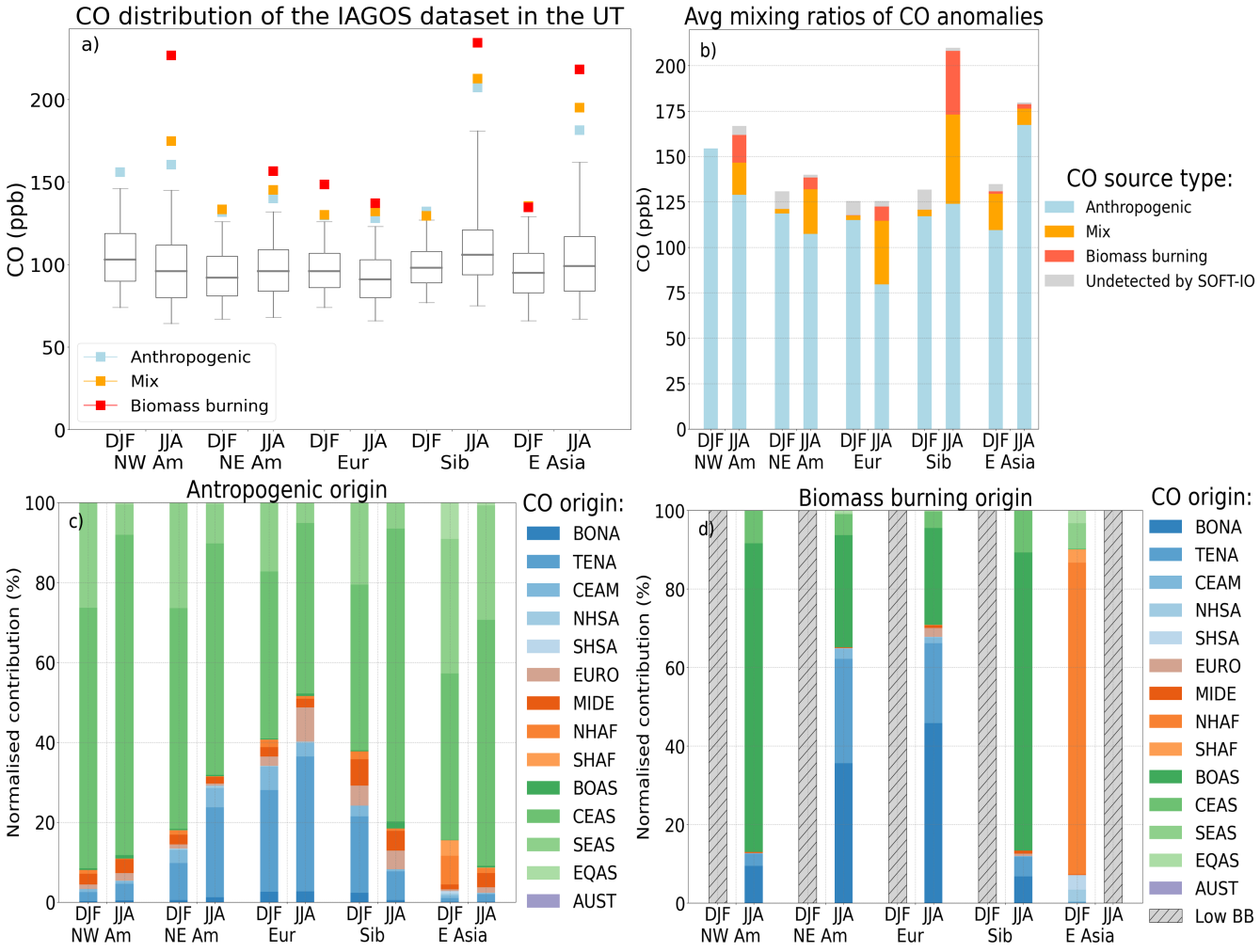

Figure 7. Same as Fig.3 but for the UT (between 8000m and the dynamical tropopause (2PVU)). At this altitude 223 anomalies over the 7865 observed are undetected by SOFT-IO, representing thus 2.8% percent (in grey on panel b).

Fig.7 is the same as Fig.3 for the upper tropospheric layer. Some regions like Europe, do not show significant variations of their 95th percentile between JJA and DJF, while other regions, like Siberia and East Asia present a drastic increase during JJA.

We can see in Fig.7.b that in DJF, the majority of the plumes are explained by anthropogenic emissions. In JJA, the number of anomalies attributed to BB increases with the onset of the northern hemisphere fire season. However, a higher number of anomalies are still explained by anthropogenic emissions, which is different from what we observe in the MT of America and Europe. This is due to the fact that the most intense pyroconvection episodes, which involve direct emission into the UT, are rare (Labonne et al., 2007). Thus, regardless of the emission intensity, vertical transport is required for a CO plume to reach the UT. Anthropogenic emissions continuously inject CO into the boundary layer. Consequently, episodes of significant vertical transport of airmasses from the surface to the UT may cause a drastic increase in the upper tropospheric CO mixing ratios,

even if local emissions are not higher than usual. However, due to the intensity of BB emissions, when these plumes reach the UT, they often are the most intense CO anomalies (Fig. 7.a). The most intense anomalies are detected in north-western America, Siberia (and East Asia in small proportion) and they are attributed to emissions of biomass burning from boreal Asia. In the UT, those anomalies even if not the most frequent, are extremely intense. Siberia and East Asia both present two of the most significant amplitudes of the CO seasonal cycle. The large increase of CO in JJA in Siberia with respect to DJF can be partly attributed to the local fires. However, approximately 60% of the episodes are still related to anthropogenic emissions and around 25% are due to MIX sources. The mean mixing ratio of these episodes during the summer months, also increased significantly compared with their winter values. Furthermore, East Asia shows a similar summertime increase in the mixing ratio of its extremes without a significant number of BB plumes.

In DJF in Siberia, the anthropogenic contributions are small and there is no clear signal. In JJA however, there is a 50% increase in the anthropogenic contribution, of which 70% comes from CEAS. The low mixing ratio and contribution in winter are partly explained by the presence of the Siberian high, which prevents the export of polluted surface airmasses from the eastern part of Asia (Pochanart et al., 2004).

However, the wind direction changes with the onset of the east Asian summer monsoon. In JJA, there are strong southeasterly ascending winds that transport pollution and moisture into the upper troposphere of East Asia. These airmasses, can even reach the northern part of Siberia, which can explain the contribution of CO from CEAS during this season in Siberia. It can explain the very low number of episodes associated with fire emissions (MIX and BB) in East Asia, as heavy rainfall prevents fires in this region and the prevailing winds from the Pacific ocean are less likely to bring airmasses polluted by Siberian fires (Pochanart et al., 2004).

In the other regions (North America and Europe), the most intense anomalies remain those attributed to BB emissions and they represent around 5 to 10% of the number of anomalies. As we said previously, the BB anomalies in NW America are attributed to emissions from boreal Asian fires. In NE America and Europe those anomalies are less intense and they are attributed to fires from boreal America, boreal Asia and TEmperate North America (TENA). Most of the BB contributions are from the two boreal regions (boreal America and boreal Asia), which is probably due to the higher emissions height of those fires increasing the probability of the emitted CO reaching the UT (Dentener et al., 2006).

In the two regions of North America, the main anthropogenic contributions to CO anomalies come from CEAS, but it can be seen that the influence of American emissions is greater in the eastern part, while the contributions in the western part originate almost entirely from CEAS. Europe's anthropogenic contributions come from Asia and North America. Only a small fraction is emitted locally, which is not surprising given the relatively weak convective activity in the region (Stohl et al., 2002).

The most polluted airmasses in the UT are often rapidly transported upward after their emission (Huang et al., 2012). Among the emitting regions, Eastern Asia is one of the more prone to vertical uplift of its pollutants because of the convective activity of the regions (WCB, east Asian monsoon...) (Stohl et al., 2002) and the presence of the Tibetan plateau, which can play an important role by lofting polluted airmass into the upper part of the troposphere (Bergman et al., 2013; Pan et al., 2016). Once in the UT, those airmasses can be transported around the hemisphere, which can be seen by the anthropogenic contribution from SOFT-IO where CEAS alone accounts for at least 40% of the anthropogenic contribution in the different regions and even

reaches 79% in NW Am. The total emissions of CEAS during this period account for about half of the northern hemisphere emissions.There is significant vertical uplift also in North America because of frequent deep convection episodes and the mid-latitude cyclone starting in the regions (Cooper and Parrish, 2004). The European region in contrast, is identified to have few vertical uplift pathways (Huntrieser and Schlager, 2004). It means that "high level" of emissions are not the only parameter to take into account, but there is also the fact that the east Asian atmosphere is characterised by strong convective activity (e.g Stohl et al. (2002)), which allows the polluted air to be quickly transported in the MT or UT where it can be distributed all over the northern hemisphere.

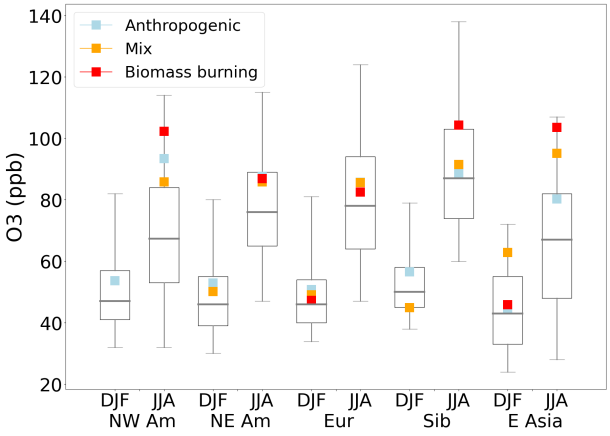

Figure 8. Same as Fig.4 for the UT.

Mixing ratios of O_3 within CO anomalies are shown in Fig. 8. As explained in sect. 2, the UT is defined as being below the 2 PVU surface. It may therefore include some stratospheric air or at least part of the mixing layer. The O_3 values measured within CO anomalies shown in Fig. 8 are mostly typical of tropospheric values, but it is possible that a small fraction of them are contaminated by some stratospheric airmasses. O_3 presents a stronger seasonal cycle than CO (Fig. 8). In DJF, the O_3 mixing ratio is at its minimum and values within the CO anomalies are slightly lower than the 75th percentile in most regions. However, during the summer months there is significant regional variations. Some regions show values of O_3 between the 75th and 95th percentile inside the CO anomalies whereas in Europe for example, the O_3 values are just above median level.

Previous studies already noticed the O_3 maximum over Siberia (Gaudel et al., 2018). (Cohen et al., 2018) suggested that this maximum could be due to a higher stratospheric influence over the region. In the anthropogenic CO anomalies, the O_3 values are close to the background. However, as demonstrated in Fig.7 a significant portion of polluted airmasses is transported from the surface of East Asia to the UT of Siberia via the East Asian summer monsoon, which could potentially influence the production of O_3.

On average for the other regions, O_3 mixing ratios in CO anomalies are 13 ppb ppb higher than their respective median and this difference can reach 21 ppb for the CO anomalies associated with biomass burning emissions. The CO anomalies with the highest values of O_3 are the anomalies associated with BB emissions from boreal Asia and detected in NW America, East

Asia and Siberia. One reason for these high ozone levels is that those anomalies all come from Siberia, a region with very high ozone levels. Moreover, we saw that those fires were responsible for particularly intense CO anomalies and so probably emitted not only CO but also many reactive compounds such as VOCs and NOx which are other precursors of O_3. As for episodes associated with anthropogenic emissions, their associated mixing ratios of O_3 are often above median levels but a lot of variation can be observed depending on the region. In NW America, in JJA levels of O_3 inside the anthropogenic CO anomalies are high (93ppb so 10ppb above its 75th percentile), those anomalies are associated with emission from CEAS, so the airmass rich in pollutants had the time to produce a significant quantity of O_3 before reaching the American continent. Production or elevated values of O_3 during the transport of polluted plumes from East Asia have already been observed during the Intercontinental Transport and Chemical Transformation 2002 campaign (ITCT 2K2) (Nowak et al., 2004; Hudman et al., 2004), so similar processes could be at play here.

3.2 India

The seasonal cycle of CO over India is characterised by a minimum in JJA in the LT and MT, and a maximum in SON-DJF in the LT, superposed by a maximum in MAM in the MT (Fig.D1 and D2 in the appendix). The Asian monsoon has a strong influence in this part of the world on the redistribution of the pollutants emitted at the surface (Lawrence, 2004b). Interesting and specific features appear in all four seasons in the UT as highlighted in Fig.9. DJF and MAM have a similar signal in the UT as the same sources are at the origin of most of the CO anomalies. We can see on Fig.9.b that half of the CO anomalies are linked to BB emissions (pure BB and MIX sources) and half are pure anthropogenic anomalies. From December until late March, it is the fire season in the northern hemisphere of Africa, and we can see on Fig.9.d that those emissions can reach the UT of India. It is also the period of the winter monsoon in Southern Asia. This season is characterised by week convective activity and northern prevailing wind, transporting pollution at low altitude toward the Indian ocean (Lelieveld et al., 2001; Lawrence and Lelieveld, 2010). Consequently, explaining the relatively high values of CO in the LT and MT during this period (Fig.D1 and D2 in the appendix), as well as the low contribution from SEAS in the UT. In the UT, the anthropogenic CO anomalies receive an influence from CEAS and SEAS but also from NHAF. In JJA, it is the wet phase of the monsoon in India so the convective activity and precipitation associated with this period (Kar et al., 2004) leads to rapid transport of the South-Asian emission to the UT while preventing BB: almost all the CO anomalies are caused by anthropogenic emissions from India or the close proximity (SEAS and CEAS). In SON, the CO anomalies are at their maximum and are caused by anthropogenic emissions from SEAS and CEAS but also by BB emissions from EQAS. The BB anomalies are clearly the most intense during this season. It is interesting to note that in the vast majority the BB anomalies recorded by IAGOS during SON were from 2015. This year was hit by a strong El Niño phenomenon characterised by especially intense fires over the Equatorial part of Asia (Field et al., 2016). According to Kar et al. (2004), during this season in 2002 there was also significant transport of CO from tropical fires.

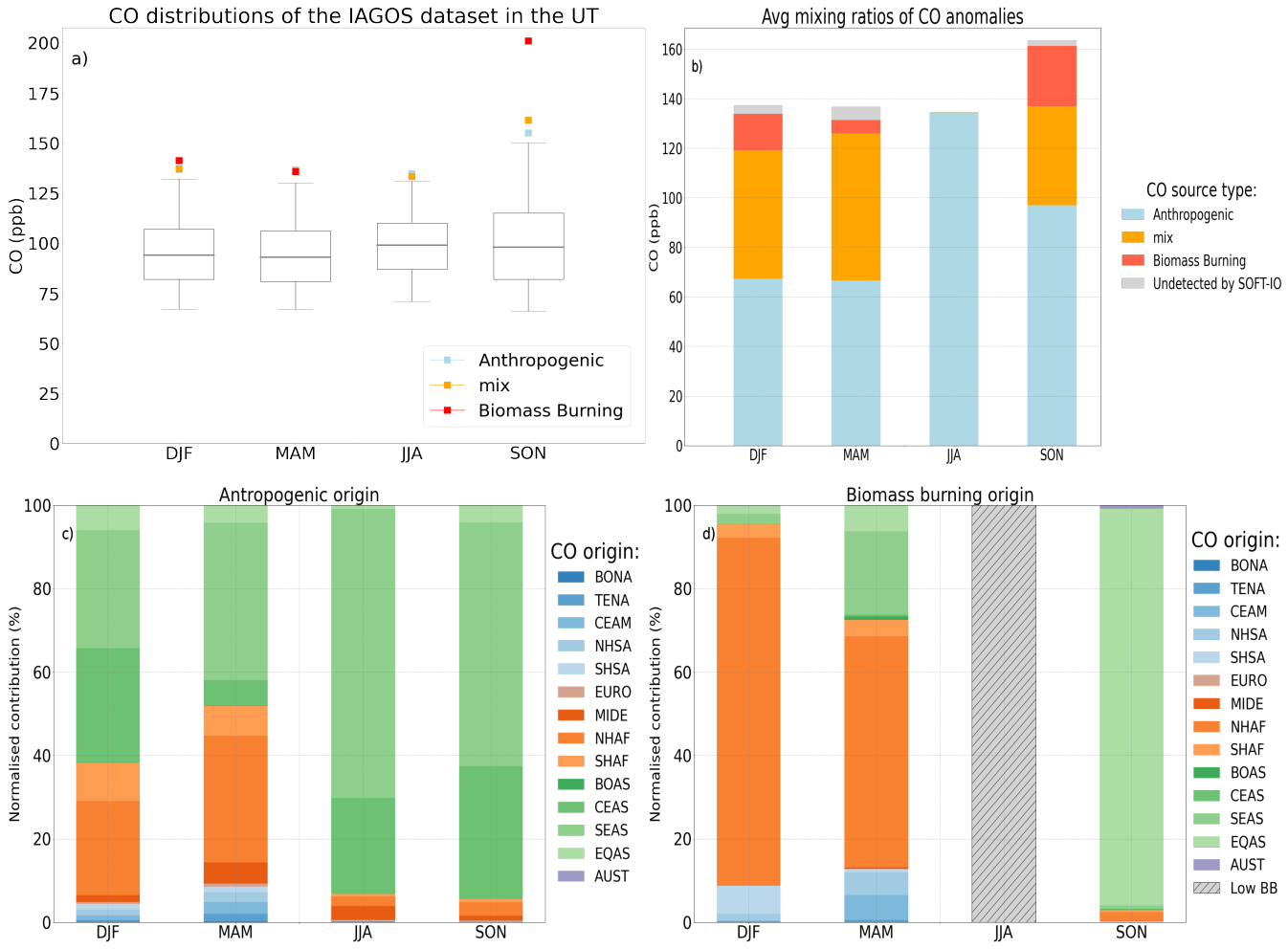

Figure 9. Same as Fig.3 but only for the Indian region during the four seasons for the UT (between 8000m and the dynamical tropopause). (In MAM in panel a) the other squares are superposed below the one from BB origins). At this altitude 37 anomalies over the 2228 observed are undetected by SOFT-IO, representing thus 1.7% (in grey on panel b).

The O_3 cycle shown here is similar to the cycle described in Lal et al. (2014). In the LT (see Fig.D3 in the appendix), the minimum values of O_3 are reached during the summer monsoon in JJA. The low values can be explained by the increased marine influence during this period (Lawrence and Lelieveld, 2010). At this altitude, the O_3 values recorded simultaneously as the CO anomalies are low and show the low O_3 production in those plumes.

385 In the MT (see Fig.D4 in the appendix) and UT (see Fig.10), the maximum of the O_3 is reached during MAM, and the minimum is reached during DJF. In the UT, in DJF and MAM a part of the CO anomalies come from northern African BB. Those plumes are associated with higher values of O_3 (11 and 10 ppb above the median respectively for DJF and MAM). CO anomalies in JJA are caused by the local emission of anthropogenic CO rapidly transported to the UT by the strong convective

activity of the South Asian summer monsoon. This rapid transport could explain that the associated values of O_3 are close to the median (65 ppb). In the post monsoon season (SON) BB anomalies from Equatorial Asia are added to the local anthropogenic anomalies. The values of O_3 in the BB plumes are low and close to the 25th percentile (44 ppb) which is explained by the lower background values of O_3 in Equatorial Asia compared to India (Cohen et al., 2018).

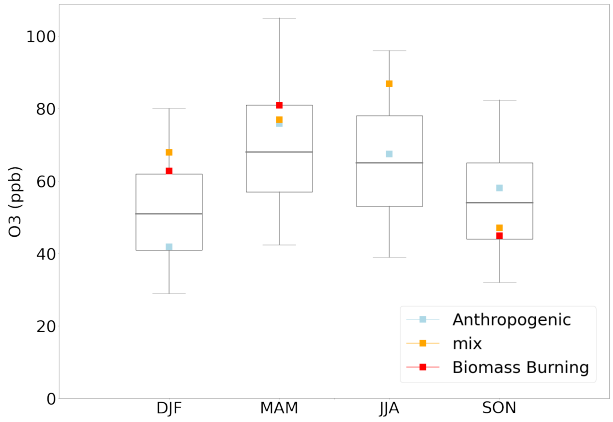

Figure 10. Same as Fig.4 for the UT in the Indian region during the four seasons.

3.3 Africa and Middle East

3.3.1 Lower and Middle Troposphere

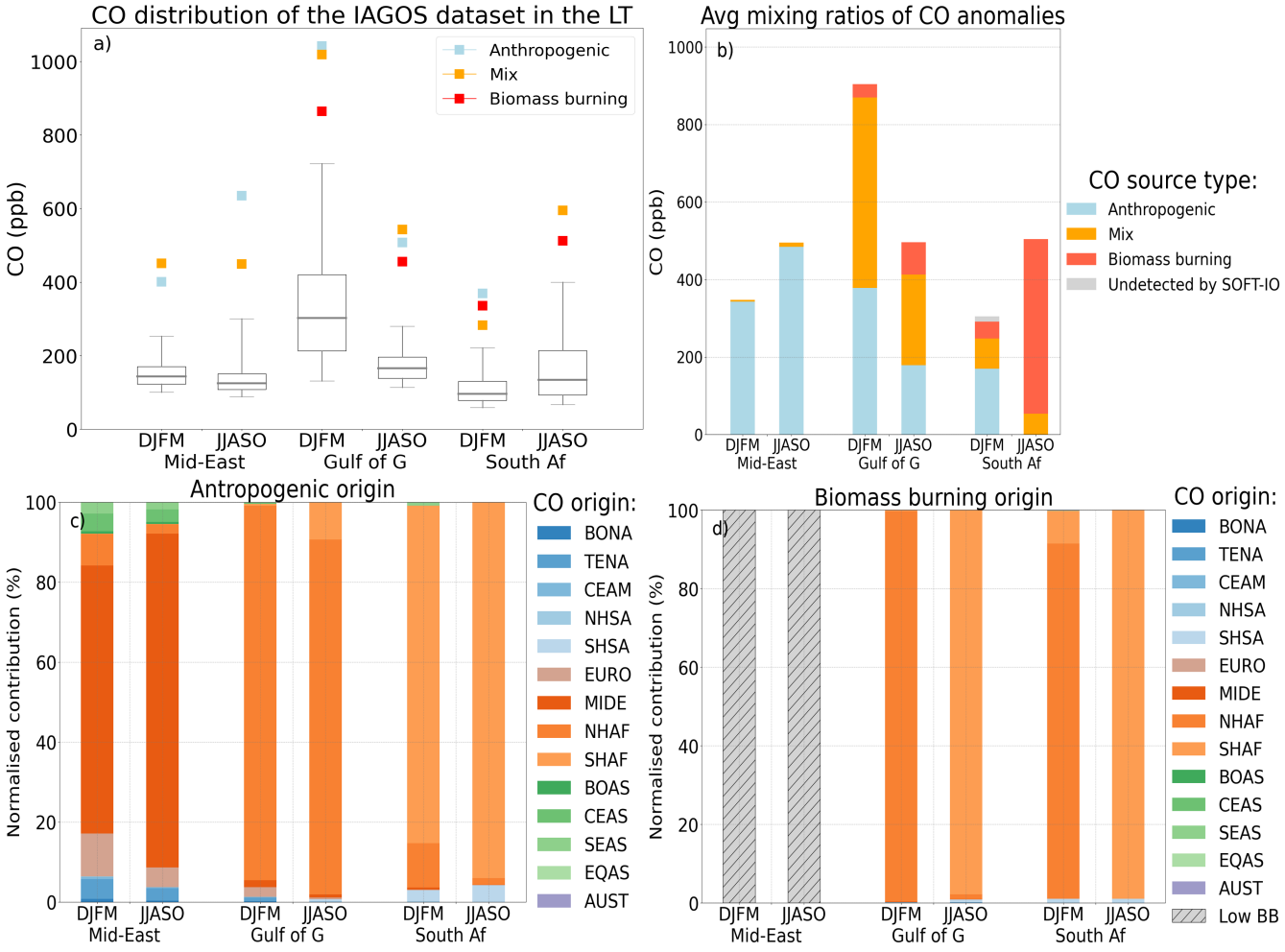

Figure 11. Same as Fig.3 but for the LT (below 2 000m) in Africa and Middle East. At this altitude 3 anomalies over the 1449 observed are undetected by SOFT-IO, representing thus 0.2% (in grey on panel b).

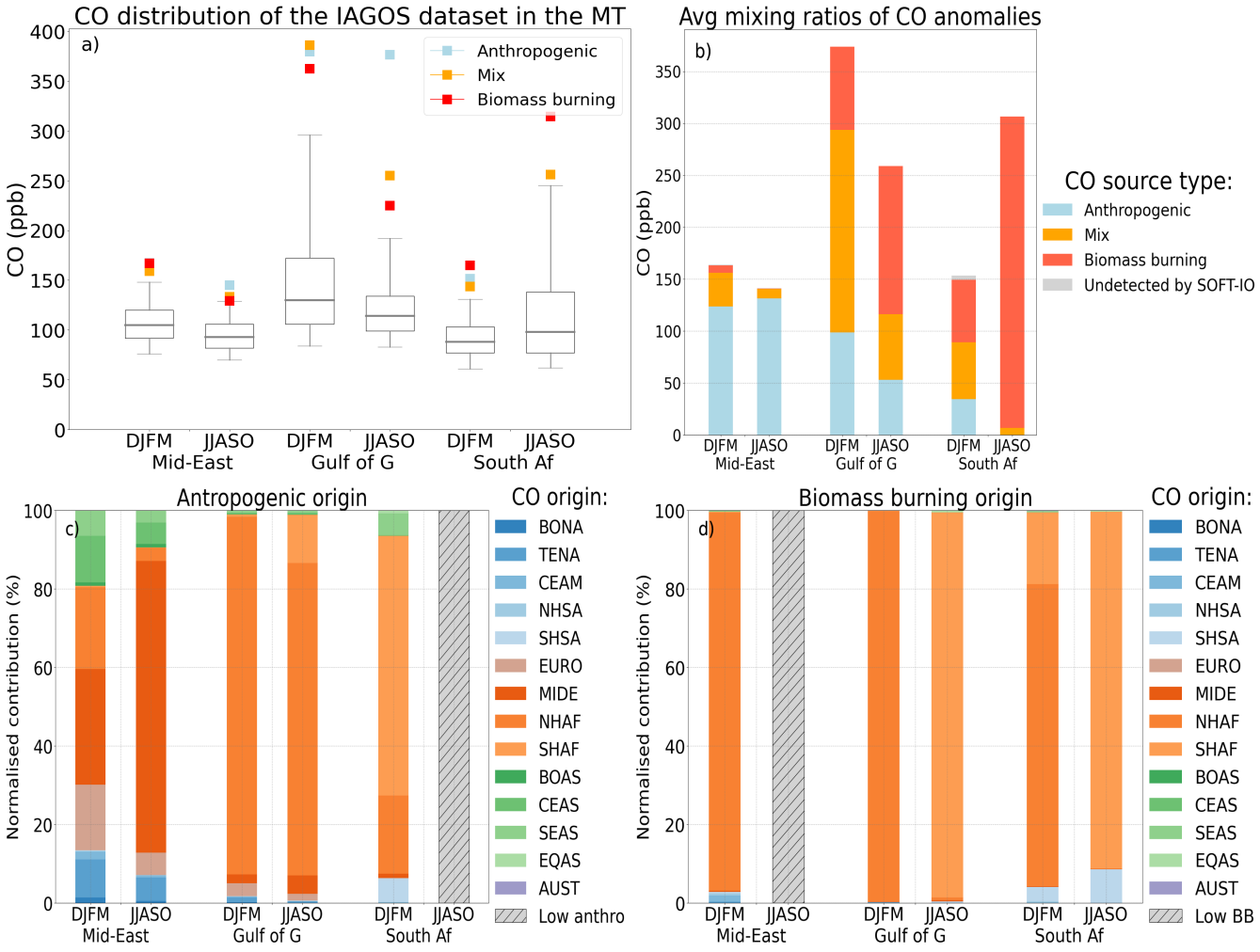

Figure 12. Same as Fig.3 but for the MT (between 2 000m and 8 000m) in Africa and Middle East. At this altitude 8 anomalies over the 1528 observed are undetected by SOFT-IO, representing thus 0.5% (in grey on panel b).

395 This section is focused on the CO anomalies detected over Africa and Middle East. As the result in the LT and in the MT present similar characteristics they are treated simultaneously.

Fig.11.a and Fig.12.a show the CO distribution in the two regions of Africa (Gulf of Guinea and Southern Africa) and the Middle East in the LT and the MT. Both layers present a maximum in DJFM in the Gulf of Guinea with a 95th percentile above 724 ppb in the LT and 297ppb in the MT. DJFM is the dry season in the northern part of Africa, which causes high levels of CO
400 from biomass burning emissions (see Fig. 11.c). In the Gulf of Guinea, the maximum values of CO are reached during DJFM, which come from the biomass burning episode of the region during this season. There is also a large population which explains the significant anthropogenic contribution. The accumulation of the pollution observed in the LT during this season has already been characterised in Sauvage et al. (2005) and is caused by the Harmattan winds. It brings rich CO airmasses caused by the

upwind fires to the southwest of the Gulf of Guinea where there are most of the airports visited by IAGOS aircrafts (see Fig.B3 in the appendix).

In JJASO, the southwesterly trade winds bring airmasses from the Atlantic ocean. These airmasses are cleaner with respect to anthropogenic pollution but can bring BB plumes from Southern Africa.

The proportion of BB sources increased in the MT. The contribution of anthropogenic emissions maximise near the surface, especially over the Gulf of Guinea, one of the largest populated and polluted urban areas of the continent. In the mid-troposphere (MT), the intensity of the CO anomalies attributed to anthropogenic sources decreases in favour of those from BB and MIX sources.

The changes in origins of the BB contributions in DJFM and JJASO follows the shift of the biomass burning season from the northern hemisphere to the southern hemisphere.

In JJASO, during the dry season in southern Africa, the anomalies are the most intense there. The MT 95th percentile is just below 250 ppb in JJASO and most of the detected anomalies of Southern Africa are attributed to emissions from southern hemisphere fires.

The Middle East plumes have a high contribution from anthropogenic emissions during both seasons, in the LT and the MT. The Middle East has been identified in previous studies as receiving the pollution of multiple regions (Li et al., 2001; Stohl et al., 2002; Duncan et al., 2008). Europe is mostly exporting its pollution via low altitude pathways and we can see on Fig 11.c and Fig 12.c that up to 20 % of the anthropogenic contributions can come from Europe. There are also contributions from Temperate North America and South and East Asia, but contrary to the European contributions these probably followed higher altitude pathways before sinking to the MT or LT (Li et al., 2001; Stohl et al., 2002). We can also see significant differences in the provenance of the anthropogenic contributions between DJFM and JJASO.

In JJASO, we are seeing contributions mostly from the local regions (MIDE) similarly to the contributions in the LT. According to previous studies the planetary boundary layer in this region can reach 4000 or 5000 meters in JJA (Gamo, 1996; Ntoumos et al., 2023). So, this differences in the origins of the contributions between DJFM and JJASO may be caused by the higher boundary layer height in JJASO.

Fig.13 and Fig.14 show the O_3 distribution measured by IAGOS as well as its mixing ratio inside the detected CO anomalies. In the following paragraph, if not mentioned otherwise, the O_3 mixing ratio refers to the mixing ratio inside the CO anomalies. The box plot Fig.13 shows that the lower part of the troposphere presents strong variability between regions and seasons.

In the Middle East, O_3 values are among the highest in JJASO in the LT and MT. The summertime median is also higher than the median from East Asia (see Fig.4 and Fig.6) which is a region with identified extreme O_3 values (Chang et al., 2017a; Lu et al., 2018). Li et al. (2001) suggested that the high tropospheric O_3 values in Middle East were due to the constant import of pollution from different regions trapped in the upper level anticyclone. The strong subsidence associated to it cause an accumulation of the O_3 in the region. Here, the CO anomalies detected are mostly caused by emissions from the Middle east rather than from long range transport. In the Middle East LT, values of O_3 inside CO anomalies attributed to anthropogenic emissions are lower than the 25th percentile, which is similar to the observation made on the northern hemisphere mid-latitudes. In the MT, the anthropogenic anomalies are close to the median during both seasons.

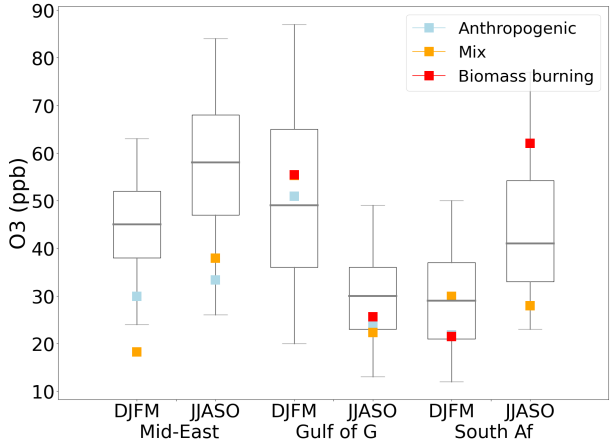

Figure 13. Same as Fig.4 for the LT in Africa and Middle East.

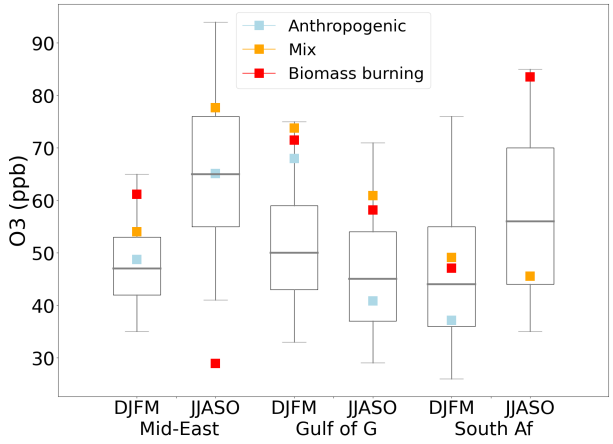

Figure 14. Same as Fig.4 for the MT in Africa and Middle East.

In DJFM, in the Gulf of Guinea, values of O_3 associated with the CO anomalies are just above the median in the LT, whereas they are almost as high as the 95th percentile in the MT. In JJASO, values of O_3 in the Gulf of Guinea exceed the median only during the MIX and BB anomalies in the MT. South Africa presents low values of O_3 in DJFM but much higher values during the BB season of the southern hemisphere. As in the northern hemisphere, the mixing ratio of O_3 inside plumes of CO influenced by BB is higher than the median. The high mixing ratio of O_3 in the BB anomalies were already discussed previously for the NH mid latitude CO anomalies. They can be caused by the high quantity of reactive gases acting as O_3 precursors emitted by biomass burning (e.g. Galanter et al. (2000); Mauzerall et al. (1998)).

3.3.2 Upper troposphere

As the seasonality of CO in the African upper troposphere has already been described in Lannuque et al. (2021), this section will emphasise the differences between the seasonal cycle of CO presented in Lannuque et al. (2021) and the extreme values of CO presented here.

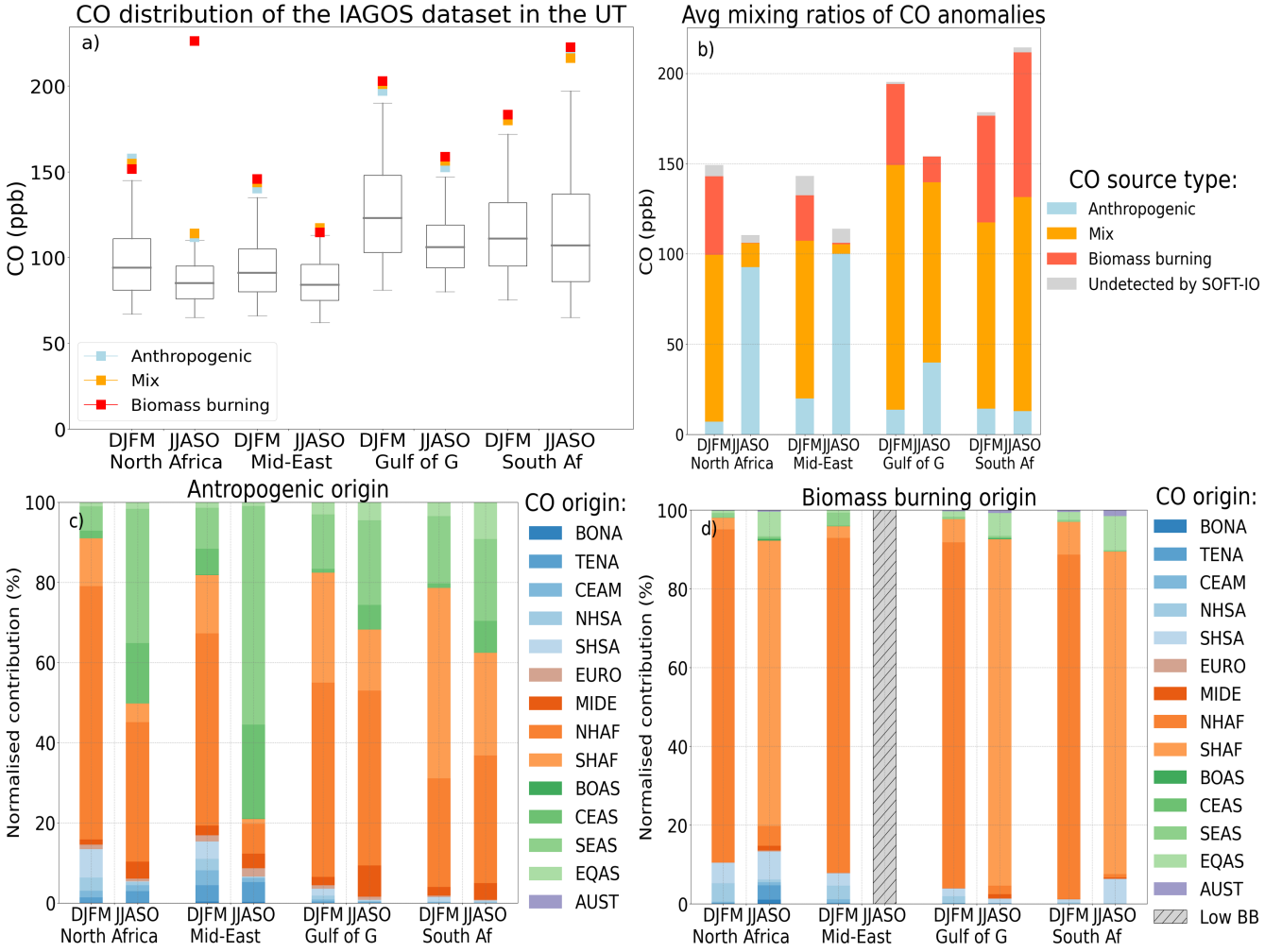

Figure 15. Same as Fig.3 but for the UT (between 8000m and the dynamical tropopause) in Africa and Middle East. At this altitude 268 anomalies over the 5859 observed are undetected by SOFT-IO, representing thus 4.6% (in grey on panel b).

Similar to the study of the CO seasonal cycle from Lannuque et al. (2021), the anomalies are the most intense in the hemisphere of the strongest Hadley cell. In DJFM, the dry season is in the African northern hemisphere causing fires emitting a lot of CO, whereas in JJASO, the dry season is in the southern hemisphere and the most intense CO anomalies are detected in South Africa.

The Middle East and the north of Africa, similarly to the Gulf of Guinea show significant seasonal variations with a maximum in DJFM. Fig.15.b shows that the DJFM maximum reached in the northern hemisphere regions are mostly caused by biomass burning plumes from NHAF (Fig. 15.d). In JJASO, it is the wet season in NHAF, so BB emissions are drastically reduced in the region. Furthermore, as Lannuque et al. (2021) showed, anthropogenic CO is transported from SEAS (Fig. 15.c). There are significant anthropogenic emissions in the Indian subcontinent, and the active convection brought by the Asian summer monsoon allows the emitted CO to be rapidly transported from the surface to the UT. There, it is trapped in the Asian monsoon anticyclone (Park et al., 2008; Barret et al., 2008; Tsivlidou et al., 2022).

Anomalies in the Gulf of Guinea and in South Africa in the UT are heavily influenced by BB emissions, only a small fraction of the plumes in these two regions are solely caused by anthropogenic emissions. The others are caused by either pure BB emissions or MIX sources. The BB contribution comes from either NHAF or SHAF depending on the season. In DJFM, in Southern Africa it is interesting to note that the CO mixing ratios are higher in the UT than in the MT (see Figs. 12 and 15 and table 1). It shows the importance of the Hadley cell circulation for the distribution of the pollutant in the UT.

The signal observed in the climatologies studied by Lannuque et al. (2021) and in the CO anomalies studied here show similarity. The main differences are the increased BB proportion from NHAF in DJFM in the four regions. The small contribution from North America observed by Lannuque et al. (2021) is barely visible here as the airmasses transported from there are probably too diluted (i.e. close to the median) to contribute to any anomalies of CO.

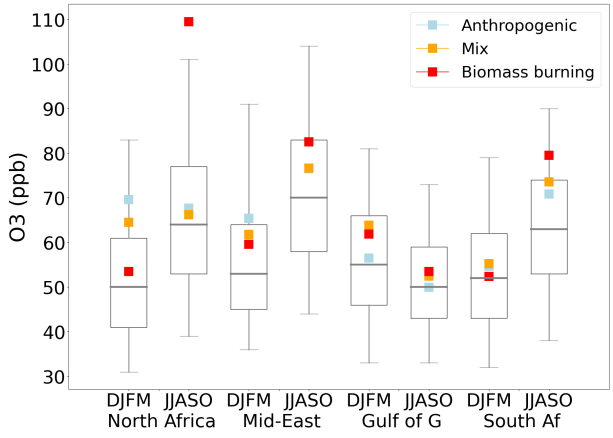

Figure 16. Same as Fig.4 for the UT in Africa and Middle East.

O_3 mixing ratio associated with the observed CO anomalies is shown in Fig.16. The upper troposphere signal is not as clear as the one from the northern hemisphere. However, like in the MT in middle East and northern Africa, we can see that the O_3 mixing ratio in the BB anomalies are higher than the median of O_3 and can even reach the 75th percentile of O_3 in DJFM. Middle East shows the highest values of O_3 during JJASO. At this altitude layer, CO anomalies are mostly from anthropogenic emissions originating from SEAS. Those anomalies show a 7 ppb enhancement compared with the median of 70 ppb. This is in agreement with a previous study from Li et al. (2001) showing elevated O_3 values in Middle East due to

significant import of anthropogenic pollution from polluted regions and very little from stratospheric intrusion. Middle East meteorological conditions are favourable for O_3 production (Duncan et al., 2008) as well as a constant import of pollutant from Asian emissions (Stohl et al., 2002) and an influx of NOx produced by lightning during the Asian monsoon Li et al. (2001).

In the Gulf of Guinea, the overall distribution of O_3 measured by IAGOS is lower than in the rest of Africa. Its maximum values of O_3 are observed in DJFM during the fire seasons of North Africa. The O_3 values observed in the CO anomalies are a bit lower than the 75th percentile in DJFM and close to the median in JJASO. In Southern Africa, in DFJM, during the raining season, no clear signal is observed. In JJASO, during the fire seasons O_3 is at its maximum and high values are observed in the CO anomalies.

3.4 Discussion on sensitivity test analysis

Our study is based on extreme CO mixing ratios, which we have defined as observations above the regional and seasonal 95th percentile. In order to ensure the robustness of the results with respect to this parameter, we performed a sensitivity test to check whether any major changes in the features could be observed with a threshold defined as the 75th or 99th percentile. Overall, the same characteristics were observed with just a few differences. In the northern hemisphere, increasing the threshold causes a slight increase in the proportion of fire-related plumes (diagnosed as BB or MIX), which is not surprising as we have seen that these plumes are the most intense most of the time.

Our study focused on CO anomalies measured between 2002 to 2019, but important trends in CO and O_3 in the atmosphere have been observed in several of the studied regions (e.g. Novelli et al. (1998); Kim et al. (2023); Gaudel et al. (2020)). So, we performed the same analysis with only the last 10 years of the IAGOS measurements. Several regions, showed a decreased 95th percentile in this datasets (see tables A2 and A3 in the appendix). However, the origins and sources of the anomalies remain similar in regions with sufficient number of data. The conclusion of the study remained largely unchanged for the CO anomalies of the last 10 years.

4 Conclusions

IAGOS is a research infrastructure which uses commercial aircraft to measure atmospheric composition. In total, over the 18 years of measurements, more than 43,000 equipped IAGOS flights were made. This study is based on the in-situ IAGOS CO anomalies defined as the observations above the 95th percentile of each individual altitude range (LT, MT, or UT), region and season. In addition, SOFT-IO allows us to give a diagnosis on the main type of source as well as the region of emission responsible for the detected CO anomalies. SOFT-IO is based on FLEXPART retro-plumes initiated at each IAGOS measurement point. The back trajectory ensembles are then coupled to two CO emissions inventories : GFAS for the biomass burning and CEDS for anthropogenic emissions. The conclusions below relate only to CO anomalies (values above the 95th percentile of the region/season/altitude).

In the northern mid-latitudes, anthropogenic emissions peak in winter, and biomass burning emissions peak in summer. In the LT, the anomalies are strongly influenced by the higher local emissions during the winter months as well as the weak

convection and low photochemical activity, which participate in the accumulation of the CO during this season. O_3 values in the CO anomalies of this season are between 8 and 23 pbb lower than the median in the different regions. In summer, at this altitude, there is significant regional variations which probably highlight the local environment more or less prone to O_3 production/destruction.

In the MT, the high CO plumes over NW and NE America, Europe in JJA are mainly due to boreal fire emissions. Those fires originate either from boreal Asia or boreal America. High CO plumes from anthropogenic origins still account for a significant proportion of the anomalies, but unlike the LT, the origins of these emissions are split between a local and a long-range influence. East Asia continues to be dominated by anthropogenic pollution throughout the year and to show the higher CO levels observed at this altitude in the northern hemisphere. O_3 in the MT in JJA, shows higher values than normal in the CO anomalies (from 7 to 9 ppb higher than the median).

In the UT, in northern mid-latitudes, anomalies caused by BB emissions remain less frequent than those from anthropogenic emissions, but they are the most intense during the boreal fire season (JJA). East asian emissions strongly influence the anomalies observed in the different regions of the northern hemisphere. The O_3 mixing ratios associated with CO anomalies are regularly higher than normal and O_3 reaches its maximum over Siberia. So, the exported CO plumes from Siberia will cause high anomalies of O_3 in the regions with lower O_3 environment.

The LT and MT of the Indian subcontinent are mostly influenced by the local anthropogenic emissions. In the UT however, the pollution pattern is dominated by the phases of the monsoon. In DJF and MAM, a significant contribution is coming from anthropogenic and BB emissions from Northern Africa. In JJA, strong convective activity favours the export of local pollution to the UT and most plumes are therefore attributed to local anthropogenic emissions. In SON, the UT above India can be strongly affected by BB emissions from in the maritime continent.

CO anomalies in the African troposphere follow a different regime. Fires are much more frequent and are responsible for a large proportion of the CO anomalies, even in the lower layers of the troposphere. The CO anomalies observed throughout the troposphere over Africa are deeply influenced by transition between the wet and dry seasons and the ITCZ shift which changes the transport patterns of the emitted CO. A part of the CO can also come from southern Asian emissions where it has been transported upward by the South Asian monsoon and trapped in the South Asian monsoon anticyclone before being transported westwards and influence the northern part of Africa and the Middle East. In the LT and MT, the maximum O_3 values are found above Middle East. Previous studies assumed that the high O_3 in the regions were due to long range transport of polluted airmasses followed by chemical production in the regions (Li et al., 2001; Duncan et al., 2008). In the African regions, O_3 levels are maximum during their respective dry season and the CO anomalies associated with BB emissions show enhanced values of O_3 (22 ppb and 28 ppb higher than the median respectively for the Gulf of Guinea and Southern Africa in the MT).

We have presented a detailed analysis of the characteristics of high carbon monoxide plumes and their associated ozone anomalies in different regions of the world. It is important for the IAGOS infrastructure to continue those measurements and to expand the regions sampled by the research infrastructure in order to provide these diagnostics in additional regions. This is particularly important in tropical regions, where anthropogenic emissions are increasing and impact on the O_3 trend globally

(Zhang et al., 2016). Increased number and sampling frequency of measurements of NOx and aerosols by IAGOS will be available and valuable for future analysis focusing on O_3 photochemical production or air quality.

Data availability. The IAGOS data (IAGOS, 2022) are available at the IAGOS data portal (https://doi.org/10.25326/20) and more precisely, the time series data are found at https://doi.org/10.25326/06 (Boulanger et al., 2018).

Acronym	Full name
BONA	BOreal North America
TENA	TEmperate North America
CEAM	CEntral AMerica
NHSA	North Hemisphere South America
SHSA	South Hemisphere South America
EURO	EUROpe
MIDE	MIDdle East
NHAF	Northern Hemisphere AFrica
SHAF	South Hemisphere AFrica
BOAS	BOreal ASia
CEAS	CEntral ASia
SEAS	South East ASia
EQAS	EQuatorial ASia
AUST	AUSTralia

Table A1. Table GFED acronym.

		LT	FT	UT
NW Am	DJF	256	160	146
	JJA	251	149	145
NE Am	DJF	264	159	126
	JJA	241	156	132
Eur	DJF	332	158	126
	JJA	200	140	123
Sib	DJF	no data	no data	127
	JJA	no data	no data	181
E Asia	DJF	559	209	129
	JJA	441	173	162

		LT	FT	UT
NW Am	DJF	224	155	142
	JJA	227	168	140
NE Am	DJF	230	148	112
	JJA	225	156	126
Eur	DJF	315	150	117
	JJA	187	135	118
Sib	DJF	no data	no data	119
	JJA	no data	no data	168
E Asia	DJF	550	205	128
	JJA	403	160	153

Table A2. q95 values (in ppb) used as thresholds for the different regions using data from 2002 to 2019 on the left and using data from 2010 to 2019 on the right.

		LT	FT	UT
India	DJF	424	157	132
	MAM	305	191	130
	JJA	267	134	131
	SON	470	150	150
North Af	DJFM	no data	no data	145
	JJASO	no data	no data	110
Middle E	DJFM	253	148	135
	JJASO	300	129	113
Gulf of G	DJFM	724	297	190
	JJASO	280	192	147
South Af	DJFM	219	132	172
	JJASO	400	245	197

		LT	FT	UT
India	DJF	399	155	131
	MAM	310	194	130
	JJA	237	132	132
	SON	468	140	155
North Af	DJFM	no data	no data	137
	JJASO	no data	no data	110
Middle E	DJFM	238	143	140
	JJASO	239	125	115
Gulf of G	DJFM	708	283	183
	JJASO	289	196	146
South Af	DJFM	252	165	162
	JJASO	457	263	195

Table A3. q95 values (in ppb) used as thresholds for the different regions using data from 2002 to 2019 on the left and using data from 2010 to 2019 on the right.

		LT	FT	UT
NW Am	DJF	168	137	88
	JJA	66	87	133
NE Am	DJF	349	323	337
	JJA	409	589	1207
Eur	DJF	1192	1032	1180
	JJA	1701	1493	2186
Sib	DJF	no data	no data	181
	JJA	no data	no data	470
E Asia	DJF	480	944	1146
	JJA	415	711	937

		LT	FT	UT
India	DJF	150	164	414
	MAM	128	121	507
	JJA	155	141	890
	SON	123	155	417
North Af	DJFM	no data	no data	433
	JJASO	no data	no data	1285
Middle E	DJFM	404	275	338
	JJASO	432	330	1282
Gulf of G	DJFM	144	303	484
	JJASO	328	269	756
South Af	DJFM	79	148	367
	JJASO	49	179	713

Table A4. Number of observed anomalies for the different regions and seasons.

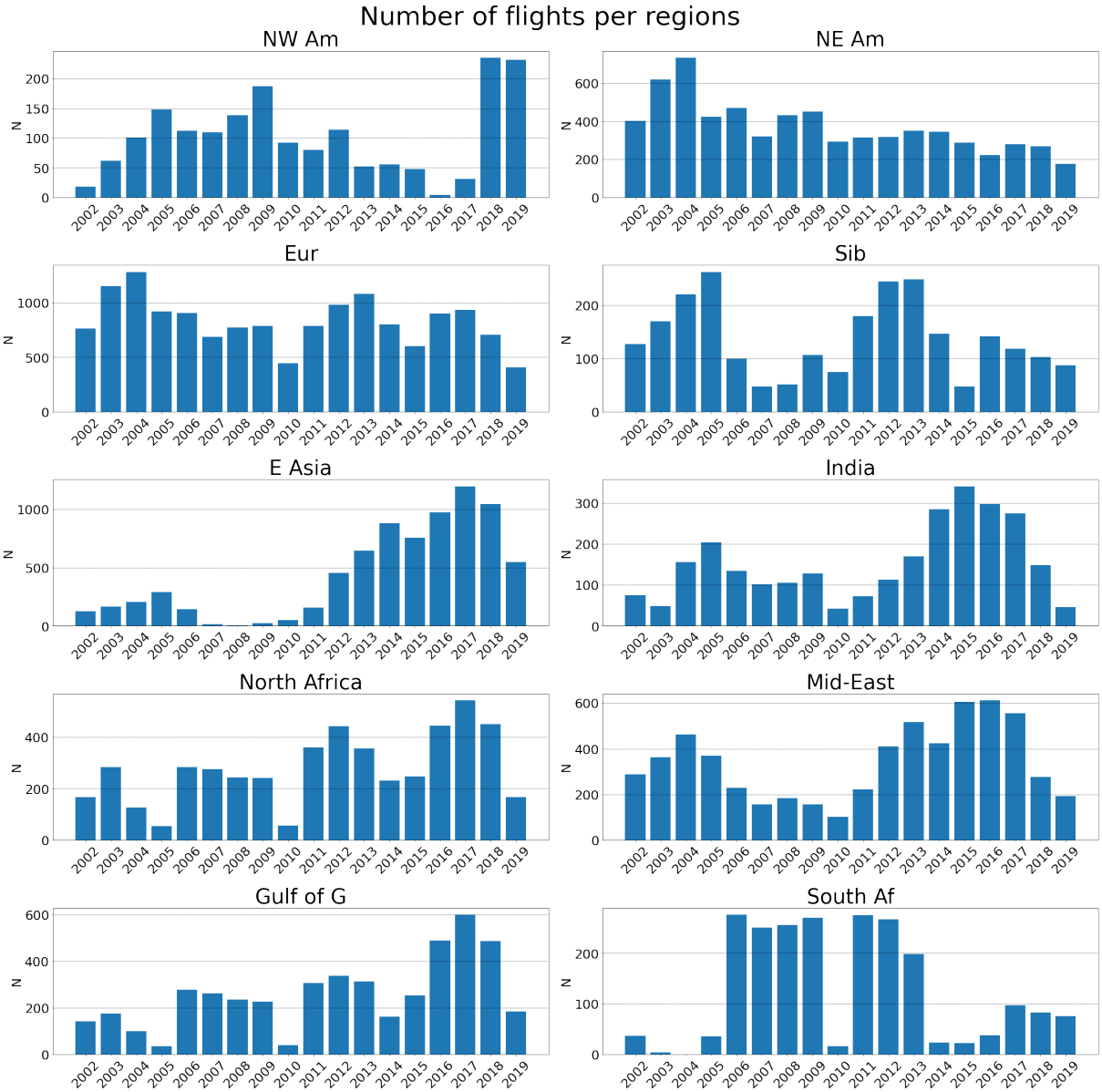

Figure B1. Data availability (number of measured flight per regions).

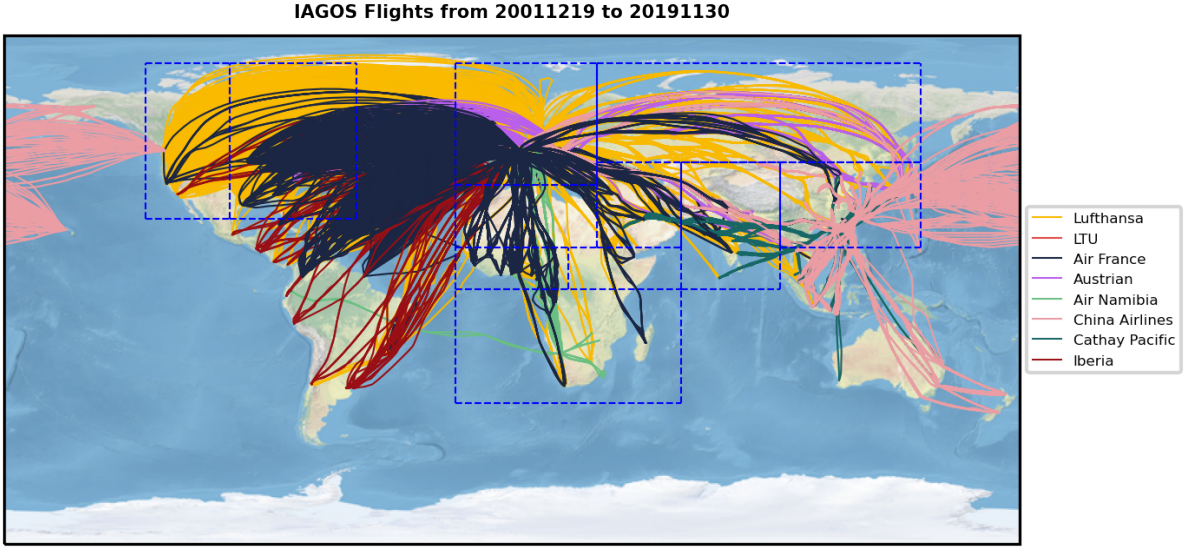

Figure B2. Trajectories of every IAGOS flight.

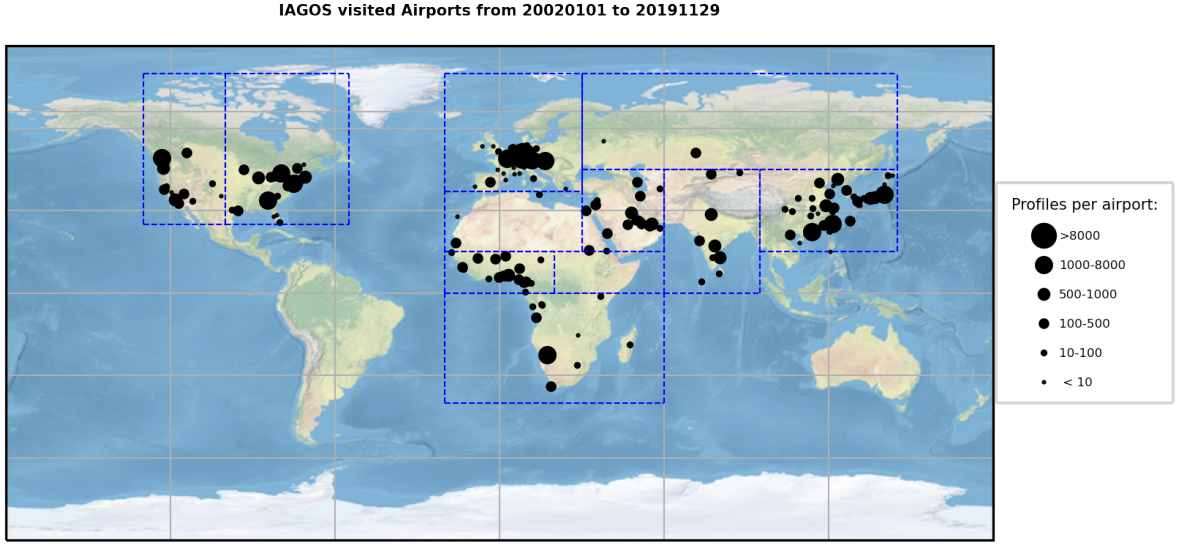

Figure B3. Number of profiles recorded per visited airport by IAGOS aircrafts.

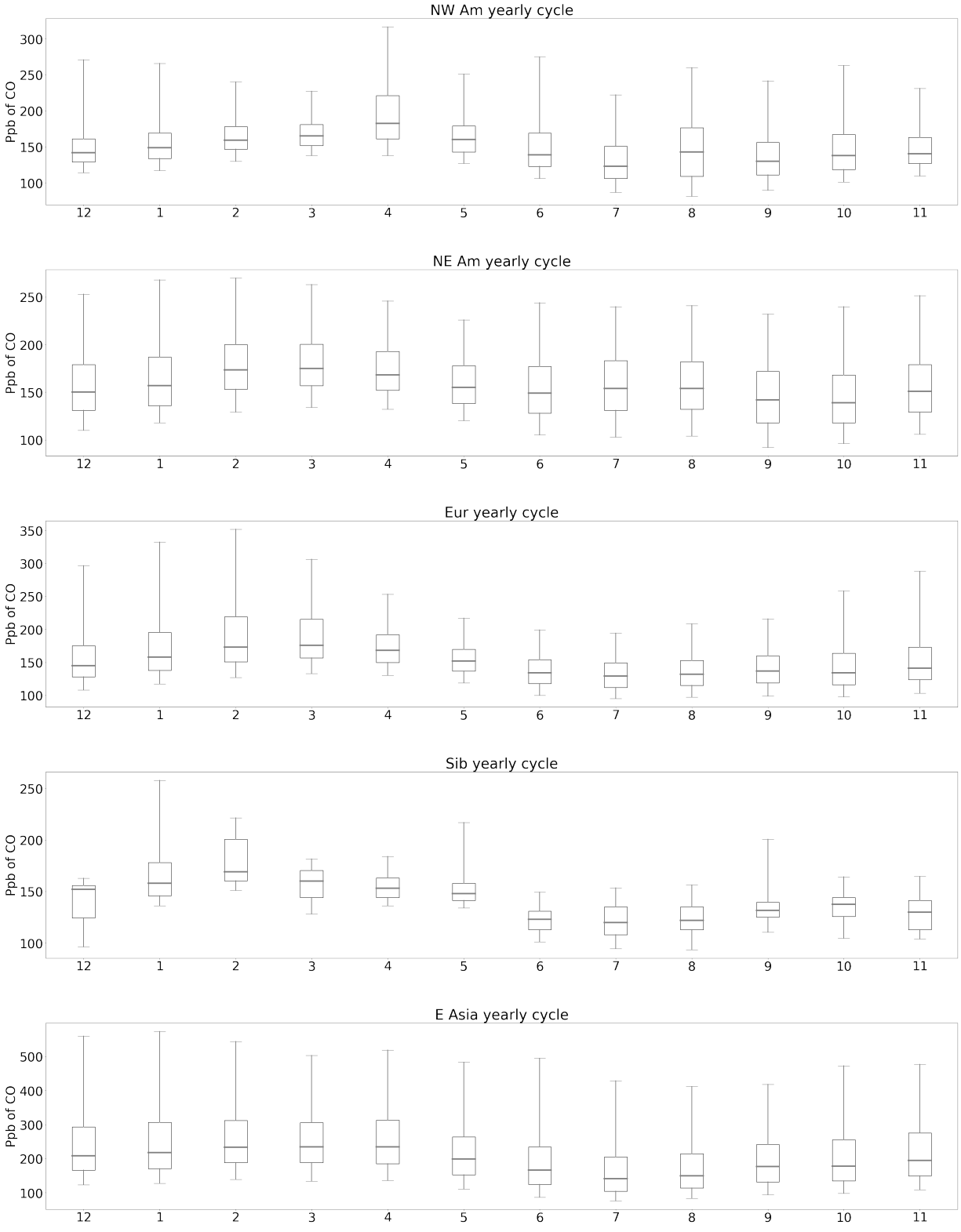

Figure C1. CO yearly cycle.

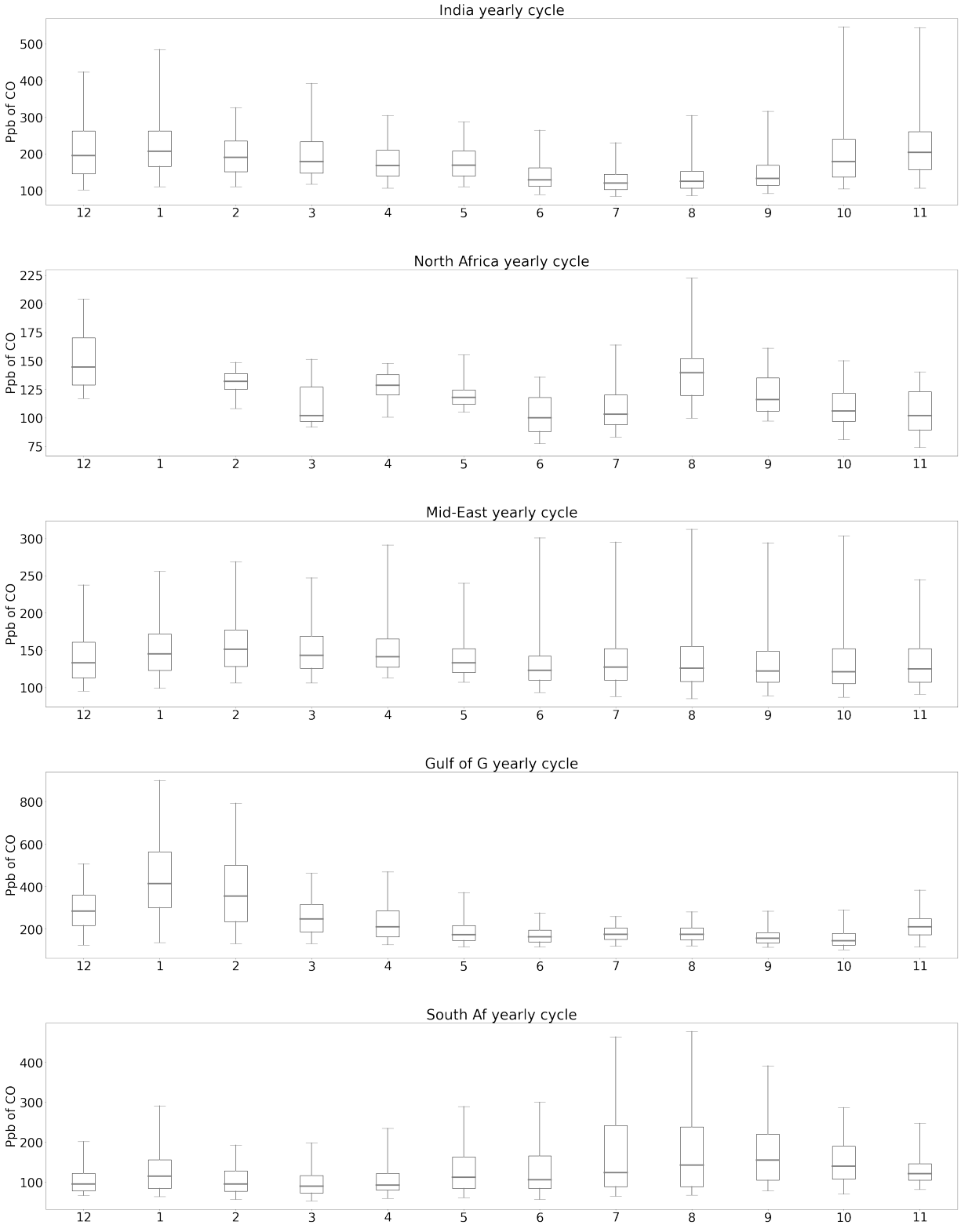

Figure C2. CO yearly cycle.

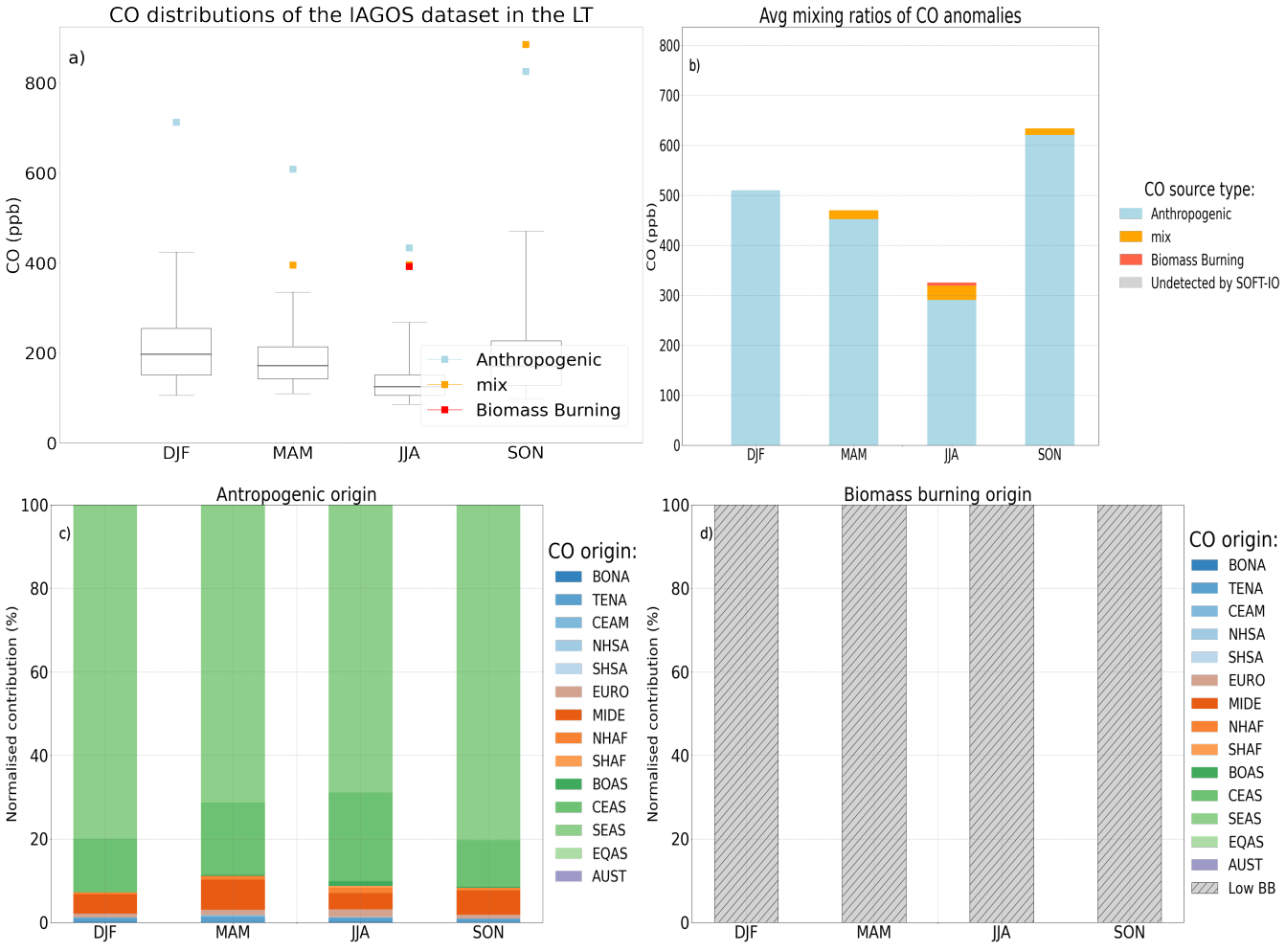

Figure D1. Same as Fig.3 but only for the Indian region during the four seasons for the LT (below 2000m). At this altitude no anomalies are undetected by SOFT-IO (in grey on panel b).

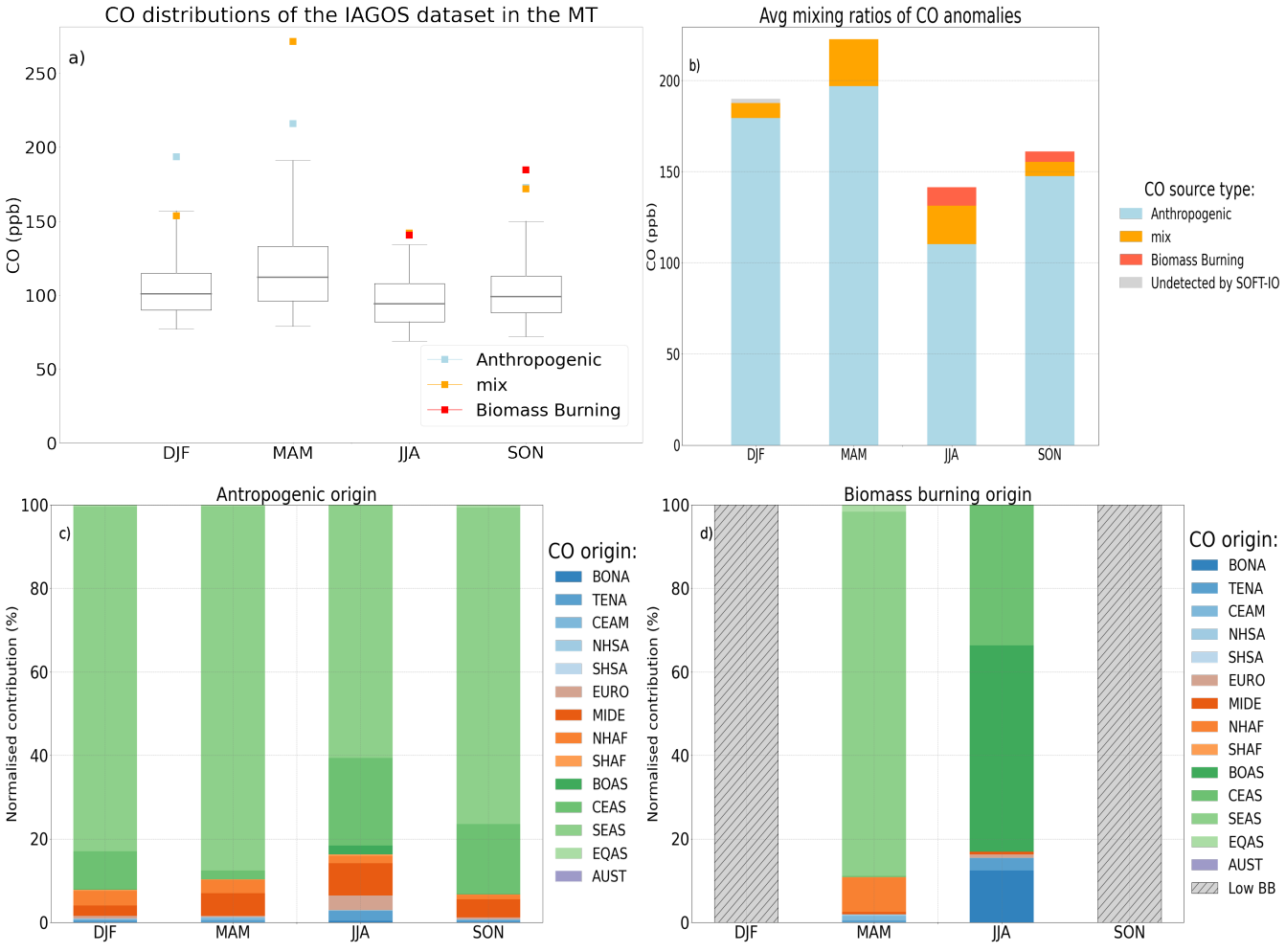

Figure D2. Same as Fig.3 but only for the Indian region during the four seasons for the MT (between 2000m and 8000m). At this altitude 2 anomalies are undetected by SOFT-IO (in grey on panel b).

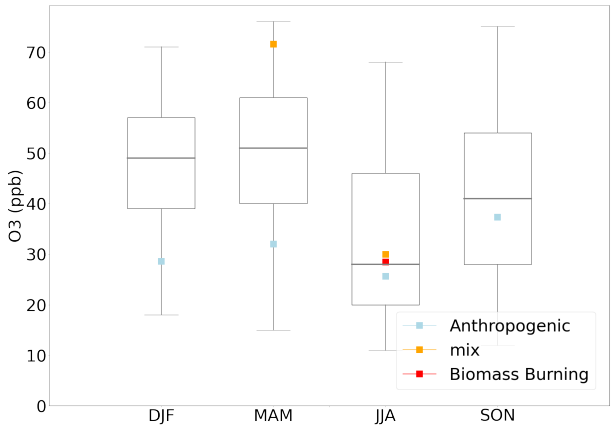

Figure D3. Same as Fig.4 for the LT in the Indian region during the four seasons.

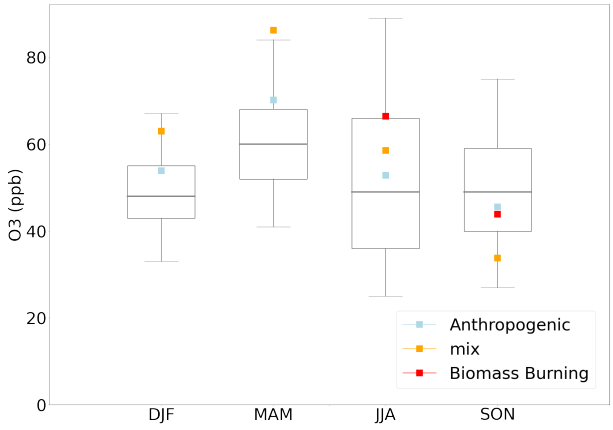

Figure D4. Same as Fig.4 for the MT in the Indian region during the four seasons.

Author contributions. TL,BS, BJ VM and VT designed the study. The IAGOS and SOFT-IO data were provided by BS, PW, YB, RB, DB, HC, JMC, PN and VT. The paper was written by TL and reviewed by BS, BJ and VT, and edited and approved by all the authors.

Competing interests. The authors declare that they have no conflict of interest.

Acknowledgements. We acknowledge the strong support of the European Commission, Airbus and the airlines (Deutsche Lufthansa, Air France, Austrian, Air Namimbia, Cathay Pacific, Iberia, China Airlines, Hawaiian Airlines, and Air Canada so far) that have carried the MOZAIC or IAGOS equipment and performed the maintenance since 1994. IAGOS has been funded by the European Union projects IAGOS–DS and IAGOS–ERI. Additionally, IAGOS has been funded by INSU-CNRS (France), Météo-France, Université Paul Sabatier (Toulouse, France) and Research Center Jülich (FZJ, Jülich, Germany). The IAGOS database is supported in France by AERIS (https://www.aeris-data.fr)

References

Andreae, M. O., Artaxo, P., Fischer, H., Freitas, S., Grégoire, J.-M., Hansel, A., Hoor, P., Kormann, R., Krejci, R., Lange, L., et al.: Transport of biomass burning smoke to the upper troposphere by deep convection in the equatorial region, Geophysical Research Letters, 28, 951–954, 2001.

Ashmore, M.: Assessing the future global impacts of ozone on vegetation, Plant, Cell & Environment, 28, 949–964, 2005.

Barret, B., Ricaud, P., Mari, C., Attié, J.-L., Bousserez, N., Josse, B., Le Flochmoën, E., Livesey, N., Massart, S., Peuch, V.-H., et al.: Transport pathways of CO in the African upper troposphere during the monsoon season: a study based upon the assimilation of spaceborne observations, Atmospheric Chemistry and Physics, 8, 3231–3246, 2008.

Barret, B., Sauvage, B., Bennouna, Y., and Le Flochmoen, E.: Upper-tropospheric CO and O 3 budget during the Asian summer monsoon, Atmospheric Chemistry and Physics, 16, 9129–9147, 2016.

Bergman, J. W., Fierli, F., Jensen, E. J., Honomichl, S., and Pan, L. L.: Boundary layer sources for the Asian anticyclone: Regional contributions to a vertical conduit, Journal of Geophysical Research: Atmospheres, 118, 2560–2575, 2013.

Blot, R., Nedelec, P., Boulanger, D., Wolff, P., Sauvage, B., Cousin, J.-M., Athier, G., Zahn, A., Obersteiner, F., Scharffe, D., et al.: Internal consistency of the IAGOS ozone and carbon monoxide measurements for the last 25 years, Atmospheric Measurement Techniques, 14, 3935–3951, 2021.

Brenninkmeijer, C., Crutzen, P., Fischer, H., Güsten, H., Hans, W., Heinrich, G., Heintzenberg, J., Hermann, M., Immelmann, T., Kersting, D., et al.: CARIBIC—Civil aircraft for global measurement of trace gases and aerosols in the tropopause region, Journal of Atmospheric and Oceanic Technology, 16, 1373–1383, 1999.

Chang, K.-L., Petropavlovskikh, I., Cooper, O. R., Schultz, M. G., and Wang, T.: Regional trend analysis of surface ozone observations from monitoring networks in eastern North America, Europe and East Asia, Elem Sci Anth, 5, 50, 2017a.

Chang, K.-L., Petropavlovskikh, I., Cooper, O. R., Schultz, M. G., and Wang, T.: Regional trend analysis of surface ozone observations from monitoring networks in eastern North America, Europe and East Asia, Elementa: Science of the Anthropocene, 5, 50, https://doi.org/10.1525/elementa.243, 2017b.

Chen, T.-M., Kuschner, W. G., Gokhale, J., and Shofer, S.: Outdoor air pollution: ozone health effects, The American journal of the medical sciences, 333, 244–248, 2007.

Cohen, Y., Petetin, H., Thouret, V., Marécal, V., Josse, B., Clark, H., Sauvage, B., Fontaine, A., Athier, G., Blot, R., et al.: Climatology and long-term evolution of ozone and carbon monoxide in the upper troposphere–lower stratosphere (UTLS) at northern midlatitudes, as seen by IAGOS from 1995 to 2013, Atmospheric Chemistry and Physics, 18, 5415–5453, 2018.

Cooper, O. R. and Parrish, D. D.: Air Pollution Export from and Import to North America: Experimental Evidence, in: Air Pollution: Intercontinental Transport of Air Pollution, edited by Stohl, A., pp. 41–67, Springer, Berlin, Heidelberg, ISBN 978-3-540-40037-0, https://doi.org/10.1007/b94523, 2004.

Cooper, O. R., Forster, C., Parrish, D., Trainer, M., Dunlea, E., Ryerson, T., Hübler, G., Fehsenfeld, F., Nicks, D., Holloway, J., de Gouw, J., Warneke, C., Roberts, J. M., Flocke, F., and Moody, J.: A case study of transpacific warm conveyor belt transport: Influence of merging airstreams on trace gas import to North America, Journal of Geophysical Research: Atmospheres, 109, https://doi.org/10.1029/2003JD003624, _eprint: https://onlinelibrary.wiley.com/doi/pdf/10.1029/2003JD003624, 2004.

Cussac, M., Marécal, V., Thouret, V., Josse, B., and Sauvage, B.: The impact of biomass burning on upper tropospheric carbon monoxide: a study using MOCAGE global model and IAGOS airborne data, Atmospheric Chemistry and Physics, 20, 9393–9417, 2020.

Damoah, R., Spichtinger, N., Servranckx, R., Fromm, M., Eloranta, E., Razenkov, I., James, P., Shulski, M., Forster, C., and Stohl, A.: A case study of pyro-convection using transport model and remote sensing data, Atmospheric Chemistry and Physics, 6, 173–185, 2006.

Davison, A. and Barnes, J.: Effects of ozone on wild plants, The New Phytologist, 139, 135–151, 1998.

Dentener, F., Kinne, S., Bond, T., Boucher, O., Cofala, J., Generoso, S., Ginoux, P., Gong, S., Hoelzemann, J., Ito, A., et al.: Emissions of primary aerosol and precursor gases in the years 2000 and 1750 prescribed data-sets for AeroCom, Atmospheric Chemistry and Physics, 6, 4321–4344, 2006.

Dickerson, R. R., Li, C., Li, Z., Marufu, L. T., Stehr, J. W., McClure, B., Krotkov, N., Chen, H., Wang, P., Xia, X., Ban, X., Gong, F., Yuan, J., and Yang, J.: Aircraft observations of dust and pollutants over northeast China: Insight into the meteorological mechanisms of transport, Journal of Geophysical Research: Atmospheres, 112, https://doi.org/10.1029/2007JD008999, _eprint: https://onlinelibrary.wiley.com/doi/pdf/10.1029/2007JD008999, 2007.

Ding, A., Wang, T., Xue, L., Gao, J., Stohl, A., Lei, H., Jin, D., Ren, Y., Wang, X., Wei, X., Qi, Y., Liu, J., and Zhang, X.: Transport of north China air pollution by midlatitude cyclones: Case study of aircraft measurements in summer 2007, Journal of Geophysical Research: Atmospheres, 114, https://doi.org/10.1029/2008JD011023, _eprint: https://onlinelibrary.wiley.com/doi/pdf/10.1029/2008JD011023, 2009.

Duncan, B. N., West, J. J., Yoshida, Y., Fiore, A. M., and Ziemke, J. R.: The influence of European pollution on ozone in the Near East and northern Africa, Atmospheric Chemistry and Physics, 8, 2267–2283, https://doi.org/10.5194/acp-8-2267-2008, publisher: Copernicus GmbH, 2008.

Fadnavis, S., Buchunde, P., Ghude, S. D., Kulkarni, S., and Beig, G.: Evidence of seasonal enhancement of CO in the upper troposphere over India, International journal of remote sensing, 32, 7441–7452, 2011.

Field, R. D., Van Der Werf, G. R., Fanin, T., Fetzer, E. J., Fuller, R., Jethva, H., Levy, R., Livesey, N. J., Luo, M., Torres, O., et al.: Indonesian fire activity and smoke pollution in 2015 show persistent nonlinear sensitivity to El Niño-induced drought, Proceedings of the National Academy of Sciences, 113, 9204–9209, 2016.

Fuhrer, J., Skärby, L., and Ashmore, M. R.: Critical levels for ozone effects on vegetation in Europe, Environmental pollution, 97, 91–106, 1997.

Galanter, M., Levy, H., and Carmichael, G. R.: Impacts of biomass burning on tropospheric CO, NO x, and O3, Journal of Geophysical Research: Atmospheres, 105, 6633–6653, 2000.

Gamo, M.: Thickness of the dry convection and large-scale subsidence above deserts, Boundary-Layer Meteorology, 79, 265–278, 1996.

Gaudel, A., Cooper, O. R., Ancellet, G., Barret, B., Boynard, A., Burrows, J. P., Clerbaux, C., Coheur, P.-F., Cuesta, J., Cuevas, E., Doniki, S., Dufour, G., Ebojie, F., Foret, G., Garcia, O., Granados-Muñoz, M. J., Hannigan, J. W., Hase, F., Hassler, B., Huang, G., Hurtmans, D., Jaffe, D., Jones, N., Kalabokas, P., Kerridge, B., Kulawik, S., Latter, B., Leblanc, T., Le Flochmoën, E., Lin, W., Liu, J., Liu, X., Mahieu, E., McClure-Begley, A., Neu, J. L., Osman, M., Palm, M., Petetin, H., Petropavlovskikh, I., Querel, R., Rahpoe, N., Rozanov, A., Schultz, M. G., Schwab, J., Siddans, R., Smale, D., Steinbacher, M., Tanimoto, H., Tarasick, D. W., Thouret, V., Thompson, A. M., Trickl, T., Weatherhead, E., Wespes, C., Worden, H. M., Vigouroux, C., Xu, X., Zeng, G., and Ziemke, J.: Tropospheric Ozone Assessment Report: Present-day distribution and trends of tropospheric ozone relevant to climate and global atmospheric chemistry model evaluation, Elementa: Science of the Anthropocene, 6, 39, https://doi.org/10.1525/elementa.291, 2018.

Gaudel, A., Cooper, O. R., Chang, K.-L., Bourgeois, I., Ziemke, J. R., Strode, S. A., Oman, L. D., Sellitto, P., Nédélec, P., Blot, R., Thouret, V., and Granier, C.: Aircraft observations since the 1990s reveal increases of tropospheric ozone at multiple locations across the Northern Hemisphere, Science Advances, 6, eaba8272, https://doi.org/10.1126/sciadv.aba8272, publisher: American Association for the Advancement of Science, 2020.

Giglio, L., Randerson, J. T., and Van Der Werf, G. R.: Analysis of daily, monthly, and annual burned area using the fourth-generation global fire emissions database (GFED4), Journal of Geophysical Research: Biogeosciences, 118, 317–328, 2013.

Huang, L., Fu, R., Jiang, J., Wright, J., and Luo, M.: Geographic and seasonal distributions of CO transport pathways and their roles in determining CO centers in the upper troposphere, Atmospheric Chemistry and Physics, 12, 4683–4698, 2012.

Hudman, R. C., Jacob, D. J., Cooper, O. R., Evans, M. J., Heald, C. L., Park, R. J., Fehsenfeld, F., Flocke, F., Holloway, J., Hübler, G., Kita, K., Koike, M., Kondo, Y., Neuman, A., Nowak, J., Oltmans, S., Parrish, D., Roberts, J. M., and Ryerson, T.: Ozone production in transpacific Asian pollution plumes and implications for ozone air quality in California, Journal of Geophysical Research: Atmospheres, 109, https://doi.org/10.1029/2004JD004974, _eprint: https://onlinelibrary.wiley.com/doi/pdf/10.1029/2004JD004974, 2004.

Huntrieser, H. and Schlager, H.: Air Pollution Export from and Import to Europe: Experimental Evidence, in: Air Pollution: Intercontinental Transport of Air Pollution, edited by Stohl, A., pp. 69–98, Springer, Berlin, Heidelberg, ISBN 978-3-540-40037-0, https://doi.org/10.1007/b94524, 2004.

IPCC: The physical science basis: Working group I contribution to the fifth assessment report of the Intergovernmental Panel on Climate Change, Stocker, T.F., D. Qin, G.-K. Plattner, M. Tignor, S.K. Allen, J. Boschung, A. Nauels, Y. Xia, V. Bex and P.M. Midgley, p. 1535, 2013.

Jaffe, D., Anderson, T., Covert, D., Kotchenruther, R., Trost, B., Danielson, J., Simpson, W., Berntsen, T., Karlsdottir, S., Blake, D., Harris, J., Carmichael, G., and Uno, I.: Transport of Asian air pollution to North America, Geophysical Research Letters, 26, 711–714, https://doi.org/10.1029/1999GL900100, _eprint: https://onlinelibrary.wiley.com/doi/pdf/10.1029/1999GL900100, 1999.

Kaiser, J., Heil, A., Andreae, M., Benedetti, A., Chubarova, N., Jones, L., Morcrette, J.-J., Razinger, M., Schultz, M., Suttie, M., et al.: Biomass burning emissions estimated with a global fire assimilation system based on observed fire radiative power, Biogeosciences, 9, 527–554, 2012.

Kar, J., Bremer, H., Drummond, J. R., Rochon, Y. J., Jones, D. B. A., Nichitiu, F., Zou, J., Liu, J., Gille, J. C., Edwards, D. P., Deeter, M. N., Francis, G., Ziskin, D., and Warner, J.: Evidence of vertical transport of carbon monoxide from Measurements of Pollution in the Troposphere (MOPITT), Geophysical Research Letters, 31, https://doi.org/10.1029/2004GL021128, _eprint: https://onlinelibrary.wiley.com/doi/pdf/10.1029/2004GL021128, 2004.

Kim, S.-W., Kim, K.-M., Jeong, Y., Seo, S., Park, Y., and Kim, J.: Changes in surface ozone in South Korea on diurnal to decadal timescales for the period of 2001–2021, Atmospheric Chemistry and Physics, 23, 12 867–12 886, https://doi.org/10.5194/acp-23-12867-2023, publisher: Copernicus GmbH, 2023.

Labonne, M., Bréon, F.-M., and Chevallier, F.: Injection height of biomass burning aerosols as seen from a spaceborne lidar, Geophysical Research Letters, 34, 2007.

Lal, S., Venkataramani, S., Chandra, N., Cooper, O. R., Brioude, J., and Naja, M.: Transport effects on the vertical distribution of tropospheric ozone over western India, Journal of Geophysical Research: Atmospheres, 119, 10 012–10 026, https://doi.org/10.1002/2014JD021854, _eprint: https://onlinelibrary.wiley.com/doi/pdf/10.1002/2014JD021854, 2014.

Lannuque, V., Sauvage, B., Barret, B., Clark, H., Athier, G., Boulanger, D., Cammas, J.-P., Cousin, J.-M., Fontaine, A., Le Flochmoën, E., et al.: Origins and characterization of CO and O 3 in the African upper troposphere, Atmospheric chemistry and physics, 21, 14 535–14 555, 2021.

Lavaysse, C., Naumann, G., Alfieri, L., Salamon, P., and Vogt, J.: Predictability of the European heat and cold waves, Climate Dynamics, 52, 2481–2495, 2019.

Lawrence, M. G.: Export of air pollution from southern Asia and its large-scale effects, Air Pollution, pp. 131–172, 2004a.

Lawrence, M. G.: Export of Air Pollution from Southern Asia and its Large-Scale Effects, in: Air Pollution: Intercontinental Transport of Air Pollution, edited by Stohl, A., pp. 131–172, Springer, Berlin, Heidelberg, ISBN 978-3-540-40037-0, https://doi.org/10.1007/b94526, 2004b.

Lawrence, M. G. and Lelieveld, J.: Atmospheric pollutant outflow from southern Asia: a review, Atmospheric Chemistry and Physics, 10, 11 017–11 096, https://doi.org/10.5194/acp-10-11017-2010, publisher: Copernicus GmbH, 2010.

Lelieveld, J., Crutzen, P. J., Ramanathan, V., Andreae, M. O., Brenninkmeijer, C. A. M., Campos, T., Cass, G. R., Dickerson, R. R., Fischer, H., de Gouw, J. A., Hansel, A., Jefferson, A., Kley, D., de Laat, A. T. J., Lal, S., Lawrence, M. G., Lobert, J. M., Mayol-Bracero, O. L., Mitra, A. P., Novakov, T., Oltmans, S. J., Prather, K. A., Reiner, T., Rodhe, H., Scheeren, H. A., Sikka, D., and Williams, J.: The Indian Ocean Experiment: Widespread Air Pollution from South and Southeast Asia, Science, 291, 1031–1036, https://doi.org/10.1126/science.1057103, publisher: American Association for the Advancement of Science, 2001.

Lelieveld, J., Gromov, S., Pozzer, A., and Taraborrelli, D.: Global tropospheric hydroxyl distribution, budget and reactivity, Atmospheric Chemistry and Physics, 16, 12 477–12 493, 2016.

Li, Q., Jacob, D. J., Logan, J. A., Bey, I., Yantosca, R. M., Liu, H., Martin, R. V., Fiore, A. M., Field, B. D., Duncan, B. N., and Thouret, V.: A tropospheric ozone maximum over the Middle East, Geophysical Research Letters, 28, 3235–3238, https://doi.org/10.1029/2001GL013134, _eprint: https://onlinelibrary.wiley.com/doi/pdf/10.1029/2001GL013134, 2001.

Li, Q., Jacob, D. J., Bey, I., Palmer, P. I., Duncan, B. N., Field, B. D., Martin, R. V., Fiore, A. M., Yantosca, R. M., Parrish, D. D., Simmonds, P. G., and Oltmans, S. J.: Transatlantic transport of pollution and its effects on surface ozone in Europe and North America, Journal of Geophysical Research: Atmospheres, 107, ACH 4–1–ACH 4–21, https://doi.org/10.1029/2001JD001422, _eprint: https://onlinelibrary.wiley.com/doi/pdf/10.1029/2001JD001422, 2002.

Liang, Q., Jaeglé, L., Jaffe, D. A., Weiss-Penzias, P., Heckman, A., and Snow, J. A.: Long-range transport of Asian pollution to the northeast Pacific: Seasonal variations and transport pathways of carbon monoxide, Journal of Geophysical Research: Atmospheres, 109, 2004.

Liang, Q., Jaeglé, L., Hudman, R. C., Turquety, S., Jacob, D. J., Avery, M. A., Browell, E. V., Sachse, G. W., Blake, D. R., Brune, W., Ren, X., Cohen, R. C., Dibb, J. E., Fried, A., Fuelberg, H., Porter, M., Heikes, B. G., Huey, G., Singh, H. B., and Wennberg, P. O.: Summertime influence of Asian pollution in the free troposphere over North America, Journal of Geophysical Research: Atmospheres, 112, https://doi.org/10.1029/2006JD007919, _eprint: https://onlinelibrary.wiley.com/doi/pdf/10.1029/2006JD007919, 2007.

Liu, H., Liu, S., Xue, B., Lv, Z., Meng, Z., Yang, X., Xue, T., Yu, Q., and He, K.: Ground-level ozone pollution and its health impacts in China, Atmospheric environment, 173, 223–230, 2018.

Lu, X., Hong, J., Zhang, L., Cooper, O. R., Schultz, M. G., Xu, X., Wang, T., Gao, M., Zhao, Y., and Zhang, Y.: Severe Surface Ozone Pollution in China: A Global Perspective, Environmental Science & Technology Letters, 5, 487–494, https://doi.org/10.1021/acs.estlett.8b00366, publisher: American Chemical Society, 2018.

Marenco, A., Thouret, V., Nédélec, P., Smit, H., Helten, M., Kley, D., Karcher, F., Simon, P., Law, K., Pyle, J., et al.: Measurement of ozone and water vapor by Airbus in-service aircraft: The MOZAIC airborne program, An overview, Journal of Geophysical Research: Atmospheres, 103, 25 631–25 642, 1998.

Mauzerall, D. L., Logan, J. A., Jacob, D. J., Anderson, B. E., Blake, D. R., Bradshaw, J. D., Heikes, B., Sachse, G. W., Singh, H., and Talbot, B.: Photochemistry in biomass burning plumes and implications for tropospheric ozone over the tropical South Atlantic, Journal of Geophysical Research: Atmospheres, 103, 8401–8423, 1998.

McDuffie, E. E., Smith, S. J., O'Rourke, P., Tibrewal, K., Venkataraman, C., Marais, E. A., Zheng, B., Crippa, M., Brauer, M., and Martin, R. V.: A global anthropogenic emission inventory of atmospheric pollutants from sector-and fuel-specific sources (1970–2017): an application of the Community Emissions Data System (CEDS), Earth System Science Data, 12, 3413–3442, 2020.

Nedelec, P., Thouret, V., Brioude, J., Sauvage, B., Cammas, J.-P., and Stohl, A.: Extreme CO concentrations in the upper troposphere over northeast Asia in June 2003 from the in situ MOZAIC aircraft data, Geophysical Research Letters, 32, 2005.

Nédélec, P., Blot, R., Boulanger, D., Athier, G., Cousin, J.-M., Gautron, B., Petzold, A., Volz-Thomas, A., and Thouret, V.: Instrumentation on commercial aircraft for monitoring the atmospheric composition on a global scale: the IAGOS system, technical overview of ozone and carbon monoxide measurements, Tellus B: Chemical and Physical Meteorology, 67, 27 791, 2015.

Novelli, P. C., Masarie, K. A., and Lang, P. M.: Distributions and recent changes of carbon monoxide in the lower troposphere, Journal of Geophysical Research: Atmospheres, 103, 19 015–19 033, https://doi.org/10.1029/98JD01366, _eprint: https://onlinelibrary.wiley.com/doi/pdf/10.1029/98JD01366, 1998.

Nowak, J. B., Parrish, D. D., Neuman, J. A., Holloway, J. S., Cooper, O. R., Ryerson, T. B., Nicks Jr., D. K., Flocke, F., Roberts, J. M., Atlas, E., de Gouw, J. A., Donnelly, S., Dunlea, E., Hübler, G., Huey, L. G., Schauffler, S., Tanner, D. J., Warneke, C., and Fehsenfeld, F. C.: Gas-phase chemical characteristics of Asian emission plumes observed during ITCT 2K2 over the eastern North Pacific Ocean, Journal of Geophysical Research: Atmospheres, 109, https://doi.org/10.1029/2003JD004488, _eprint: https://onlinelibrary.wiley.com/doi/pdf/10.1029/2003JD004488, 2004.

Ntoumos, A., Hadjinicolaou, P., Zittis, G., Constantinidou, K., Tzyrkalli, A., and Lelieveld, J.: Evaluation of WRF Model Boundary Layer Schemes in Simulating Temperature and Heat Extremes over the Middle East–North Africa (MENA) Region, Journal of Applied Meteorology and Climatology, 62, 1315–1332, 2023.

Owen, R., Cooper, O., Stohl, A., and Honrath, R.: An analysis of the mechanisms of North American pollutant transport to the central North Atlantic lower free troposphere, Journal of Geophysical Research: Atmospheres, 111, 2006.

Pan, L. L., Honomichl, S. B., Kinnison, D. E., Abalos, M., Randel, W. J., Bergman, J. W., and Bian, J.: Transport of chemical tracers from the boundary layer to stratosphere associated with the dynamics of the Asian summer monsoon, Journal of Geophysical Research: Atmospheres, 121, 14–159, 2016.

Park, M., Randel, W. J., Gettelman, A., Massie, S. T., and Jiang, J. H.: Transport above the Asian summer monsoon anticyclone inferred from Aura Microwave Limb Sounder tracers, Journal of Geophysical Research: Atmospheres, 112, 2007.

Park, M., Randel, W. J., Emmons, L. K., Bernath, P. F., Walker, K. A., and Boone, C. D.: Chemical isolation in the Asian monsoon anticyclone observed in Atmospheric Chemistry Experiment (ACE-FTS) data, Atmospheric Chemistry and Physics, 8, 757–764, 2008.

Paugam, R., Wooster, M., Atherton, J., Freitas, S., Schultz, M., and Kaiser, J.: Development and optimization of a wildfire plume rise model based on remote sensing data inputs–Part 2, Atmospheric Chemistry and Physics Discussions, 15, 9815–9895, 2015.

Petetin, H., Thouret, V., Fontaine, A., Sauvage, B., Athier, G.and Blot, R., Boulanger, D., Cousin, J.-M., and Nédélec, P.: Representativeness of the IAGOS airborne measurements in the lower troposphere, Atmospheric Chemistry and Physics, 16, 2016.

Petetin, H., Jeoffrion, M., Sauvage, B., Athier, G., Blot, R., Boulanger, D., Clark, H., Cousin, J.-M., Gheusi, F., Nedelec, P., et al.: Representativeness of the IAGOS airborne measurements in the lower troposphere, Elementa: Science of the Anthropocene, 6, 2018a.

Petetin, H., Sauvage, B., Parrington, M., Clark, H., Fontaine, A., Athier, G., Blot, R., Boulanger, D., Cousin, J.-M., Nédélec, P., et al.: The role of biomass burning as derived from the tropospheric CO vertical profiles measured by IAGOS aircraft in 2002–2017, Atmospheric Chemistry and Physics, 18, 17 277–17 306, 2018b.

Petzold, A., Thouret, V., Gerbig, C., Zahn, A., Brenninkmeijer, C. A., Gallagher, M., Hermann, M., Pontaud, M., Ziereis, H., Boulanger, D., et al.: Global-scale atmosphere monitoring by in-service aircraft–current achievements and future prospects of the European Research Infrastructure IAGOS, Tellus B: Chemical and Physical Meteorology, 67, 28 452, 2015.

Pochanart, P., Wild, O., and Akimoto, H.: Air pollution import to and export from East Asia, Air pollution: Intercontinental transport of air pollution, pp. 99–130, 2004.

Qu, Z., Henze, D. K., Worden, H. M., Jiang, Z., Gaubert, B., Theys, N., and Wang, W.: Sector-based top-down estimates of NOx, SO2, and CO emissions in East Asia, Geophysical research letters, 49, e2021GL096 009, 2022.

Rémy, S., Veira, A., Paugam, R., Sofiev, M., Kaiser, J. W., Marenco, F., Burton, S. P., Benedetti, A., Engelen, R. J., Ferrare, R., et al.: Two global data sets of daily fire emission injection heights since 2003, Atmospheric Chemistry and Physics, 17, 2921–2942, 2017.

Ricaud, P., Sič, B., El Amraoui, L., Attié, J.-L., Zbinden, R., Huszar, P., Szopa, S., Parmentier, J., Jaidan, N., Michou, M., et al.: Impact of the Asian monsoon anticyclone on the variability of mid-to-upper tropospheric methane above the Mediterranean Basin, Atmospheric Chemistry and Physics, 14, 11 427–11 446, 2014.

Riese, M., Ploeger, F., Rap, A., Vogel, B., Konopka, P., Dameris, M., and Forster, P.: Impact of uncertainties in atmospheric mixing on simulated UTLS composition and related radiative effects, Journal of Geophysical Research: Atmospheres, 117, 2012.

Sauvage, B., Thouret, V., Cammas, J.-P., Gheusi, F., Athier, G., and Nédélec, P.: Tropospheric ozone over Equatorial Africa: regional aspects from the MOZAIC data, Atmospheric Chemistry and Physics, 5, 311–335, 2005.

Sauvage, B., Fontaine, A., Eckhardt, S., Auby, A., Boulanger, D., Petetin, H., Paugam, R., Athier, G., Cousin, J.-M., Darras, S., et al.: Source attribution using FLEXPART and carbon monoxide emission inventories: SOFT-IO version 1.0, Atmospheric Chemistry and Physics, 17, 15 271–15 292, 2017.

Seinfeld, J. and Pandis, S.: Atmospheric chemistry and physics. 1997, New York, 2008.

Shastri, H., Ghosh, S., and Karmakar, S.: Improving Global Forecast System of extreme precipitation events with regional statistical model: Application of quantile-based probabilistic forecasts, Journal of Geophysical Research: Atmospheres, 122, 1617–1634, 2017.

Smoydzin, L. and Hoor, P.: Contribution of Asian emissions to upper tropospheric CO over the remote Pacific, Atmospheric Chemistry and Physics, 22, 7193–7206, 2022.

Stohl, A.: A 1-year Lagrangian "climatology" of airstreams in the northern hemisphere troposphere and lowermost stratosphere, Journal of Geophysical Research: Atmospheres, 106, 7263–7279, https://doi.org/10.1029/2000JD900570, _eprint: https://onlinelibrary.wiley.com/doi/pdf/10.1029/2000JD900570, 2001.

Stohl, A., Eckhardt, S., Forster, C., James, P., and Spichtinger, N.: On the pathways and timescales of intercontinental air pollution transport, Journal of Geophysical Research: Atmospheres, 107, ACH 6–1–ACH 6–17, https://doi.org/10.1029/2001JD001396, _eprint: https://onlinelibrary.wiley.com/doi/pdf/10.1029/2001JD001396, 2002.

Stohl, A., Forster, C., Frank, A., Seibert, P., and Wotawa, G.: The Lagrangian particle dispersion model FLEXPART version 6.2, Atmospheric Chemistry and Physics, 5, 2461–2474, 2005.

Thouret, V., Marenco, A., Logan, J. A., Nédélec, P., and Grouhel, C.: Comparisons of ozone measurements from the MOZAIC airborne program and the ozone sounding network at eight locations, Journal of Geophysical Research: Atmospheres, 103, 25 695–25 720, 1998.

Thouret, V., Cammas, J.-P., Sauvage, B., Athier, G., Zbinden, R., Nédélec, P., Simon, P., and Karcher, F.: Tropopause referenced ozone climatology and inter-annual variability (1994–2003) from the MOZAIC programme, Atmospheric Chemistry and Physics, 6, 1033–1051, 2006.

Thouret, V., Clark, H., Petzold, A., Nédélec, P., and Zahn, A.: IAGOS: Monitoring Atmospheric Composition for Air Quality and Climate by Passenger Aircraft, Handbook of Air Quality and Climate Change, 18, 17 277–17 306, 2022.

Tsivlidou, M., Sauvage, B., Barret, B., Wolff, P., Clark, H., Bennouna, Y., Blot, R., Boulanger, D., Nédélec, P., Le Flochmoën, E., et al.: Tropical tropospheric ozone and carbon monoxide distributions: characteristics, origins and control factors, as seen by IAGOS and IASI, Atmospheric Chemistry and Physics Discussions, pp. 1–50, 2022.

Val Martin, M., Logan, J., Kahn, R., Leung, F.-Y., Nelson, D., and Diner, D.: Smoke injection heights from fires in North America: analysis of 5 years of satellite observations, Atmospheric Chemistry and Physics, 10, 1491–1510, 2010.

Xia, Y., Huang, Y., and Hu, Y.: On the climate impacts of upper tropospheric and lower stratospheric ozone, Journal of Geophysical Research: Atmospheres, 123, 730–739, 2018.

Yang, J., Liu, J., Han, S., Yao, Q., and Cai, Z.: Study of the meteorological influence on ozone in urban areas and their use in assessing ozone trends in all seasons from 2009 to 2015 in Tianjin, China, Meteorology and Atmospheric Physics, 131, 1661–1675, https://doi.org/10.1007/s00703-019-00664-x, 2019.

Zhang, Y., Cooper, O. R., Gaudel, A., Thompson, A. M., Nédélec, P., Ogino, S.-Y., and West, J. J.: Tropospheric ozone change from 1980 to 2010 dominated by equatorward redistribution of emissions, Nature Geoscience, 9, 875–879, 2016.